RESEARCH ARTICLE | JULY 11 2025

Pseudo-boiling of supercritical CO_2 in horizontal tubes: the influence of tube diameter Θ

Bowen Yu (于博文); Jian Xie (谢剑) ┗ [Jinliang Xu (徐进良) □ ; Qiuru Dong (董邱儒) □ ; Liangyuan Cheng (程亮元)



Physics of Fluids 37, 073324 (2025) https://doi.org/10.1063/5.0272143





Articles You May Be Interested In

Dry cooler contribution to LCOE in a sCO₂ power cycle for CSP

AIP Conf. Proc. (May 2022)

Thermomechanical modeling of counter-flow packed-bed particle-to-sCO₂ heat exchangers

AIP Conf. Proc. (May 2022)

Narrow-channel fluidized beds for particle-sCO₂ heat exchangers in next generation CPS plants

AIP Conf. Proc. (May 2022)





Pseudo-boiling of supercritical CO₂ in horizontal tubes: the influence of tube diameter

Cite as: Phys. Fluids **37**, 073324 (2025); doi: 10.1063/5.0272143 Submitted: 22 March 2025 · Accepted: 22 May 2025 ·







Published Online: 11 July 2025

Bowen Yu (于博文),¹ Jian Xie (谢剑),^{1,a)} <mark>向</mark> Jinliang Xu (徐进良),^{1,2} **向** Qiuru Dong (董邱儒),¹ **向** and Liangyuan Cheng (程亮元)¹

AFFILIATIONS

¹Beijing Key Laboratory of Multiphase Flow and Heat Transfer for Low Grade Energy Utilization, North China Electric Power University, Beijing 102206, China

²Key Laboratory of Power Station Energy Transfer Conversion and System of Ministry of Education, North China Electric Power University, Beijing 102206, China

ABSTRACT

Supercritical carbon dioxide (sCO₂) is a promising working fluid to improve the efficiency of advanced power systems. Relevant to the use of sCO₂ in parabolic trough solar receivers, heating sCO₂ in a horizontal tube is investigated numerically. The ranges of tube diameter, pressure, mass flux, and heat flux are 8-12 mm, 10-20 MPa, 700-1300 kg/m²s, and 66.7-300 kW/m², respectively. When heat transfer deterioration occurs at high heat flux, there are not only overshoot wall temperatures along the flow direction but also non-uniform wall temperatures in the circumferential direction. Temperature difference ΔT between the top and bottom generatrix of the tube wall reaches 199.7 K, maximally. To suppress ΔT , the influence of tube diameter on supercritical heat transfer is analyzed based on pseudo-boiling theory. The result shows that the heat transfer coefficient (HTC) at the top generatrix decreases while HTC at the bottom generatrix exhibits nonlinear variation with reducing diameter. Heat transfer performance at both the top and bottom generatrix is determined by the thermal resistance of a vapor-like film on the tube. It can be characterized by a supercritical K number, involving the balance of evaporation momentum force and inertia force on the vapor-like film. Thus, ΔT is determined by the ratio of K number at the tube top to that at the tube bottom and ΔT significantly decreases with reducing tube diameters. In addition, increasing pressure and mass flux can also reduce ΔT . This paper not only advances the pseudo-boiling heat transfer theory of supercritical fluids, but also provides guidance for the safety design of sCO₂ heat exchangers in advanced power systems.

Published under an exclusive license by AIP Publishing. https://doi.org/10.1063/5.0272143

I. INTRODUCTION

Increasing the efficiency of energy systems is important to suppressing global warming caused by the greenhouse effect. It is known that the system efficiency can be increased by rising the vapor temperature entering the turbine. Thus, supercritical water with high temperature and pressure has been widely used in energy systems. However, the active chemical reaction between supercritical water and solid material limits the further improvement of steam temperature and system efficiency. Recently, supercritical carbon dioxide (sCO₂) has become an alternative working fluid due to its chemical inertness, offering the opportunity to improve the cycle efficiency with higher vapor parameters. Compared with water, sCO₂ also behaves limited heat transfer performance. The heat exchangers need to be redesigned. The top priority is to determine the tube diameter according to its influence on the heat transfer performance of sCO₂.

To develop advanced boilers and nuclear reactors, the vertical upflow of sCO₂ is widely investigated. Zhao *et al.*² investigated the influence of channel size on heating sCO₂ in vertical tubes under a similar heat flux to mass flux ratio. The results demonstrated that tubes with an inner diameter of 0.27 mm exhibited deteriorated heat transfer due to flow acceleration effects, whereas tubes with an inner diameter of 2.0 mm showed improved heat transfer performance due to buoyancy effects. However, Song *et al.*^{3–5} declared that the tube with bigger diameter reduces the heat transfer coefficient (HTC) due to buoyancy, after comparing the heat transfer performance in vertical tubes with inner diameters of 4.4 and 9.0 mm. Zahlan *et al.*⁶ also reported that the HTC of sCO₂ in an 8 mm tube is slightly higher than that in the 22 mm tube. What is more, heat transfer deterioration is disposed to appear in the tube with a bigger diameter.

^{a)}Author to whom correspondence should be addressed: xiejian90@ncepu.edu.cn

Compared to sCO₂ heated in vertical tubes, sCO₂ heat transfer in horizontal tubes is seldom investigated. However, it is important for the safety design of horizontal heat exchangers in advanced sCO2 power systems, such as parabolic trough solar receiver. Liao and Zhao⁸ presented an experiment of sCO₂ heated in both vertical and horizontal tubes with inside diameters of 0.70, 1.40, and 2.16 mm. It is found that HTCs of both horizontal flow and vertical upflow exhibit similar values and trends vs mainstream temperature. The Nusselt numbers increase with rising tube diameter. However, Wang et al.9 obtained the opposite conclusion that HTC decreases with increasing tube diameter. Recently, Cheng et al. 10 performed an experiment and concluded that the heat transfer of sCO2 in horizontal tubes is nonuniform in the circumferential direction. Specifically, HTCs at the top generatrix of horizontal tube decrease with rising tube diameter, while HTCs at the bottom generatrix do not blindly decrease with the increased tube diameter. It confirms that heat transfer in the horizontal tube becomes more complex than that in the vertical tube. However, the above experiment only obtained the discrete temperature at limited locations on the tube wall. It is necessary to perform coupled fluidsolid numerical simulation to obtain temperature fields both on the tube and inside the tube. Theoretical analysis is desired to combine the above temperature fields to reveal the influence mechanism of tube diameter on sCO2 heat transfer.

The above experiments obtained different conclusions about the influence of tube diameter on sCO_2 heat transfer. It is necessary to reveal the heat transfer mechanism by theoretical analysis and numerical simulation. Traditionally, supercritical fluids were assumed as single phase. Unfortunately, there are still contradictory conclusions under the single-phase flow theory. For example, both Yu *et al.*¹¹ and Wang *et al.*¹² consider the buoyancy effect in numerical simulation, but their conclusions about the influence of tube diameter on sCO_2 heat transfer deterioration are still reversed. In fact, the buoyancy effect can be characterized by the dimensionless number Bu in the single-phase flow theory of supercritical fluids. However, it is concluded that Bu cannot identify the normal heat transfer and heat transfer deterioration. Heat Thus, the single-phase flow theory has limitations in discussing the influence of tube diameter on sCO_2 heat transfer.

Recently, extensive research efforts and investigations support that supercritical fluids exhibit an inhomogeneous structure and multiphase flow characteristics.^{17–26} Wang *et al.*²⁷ proposed a three-regime model of supercritical heat transfer based on the pseudo-boiling concept and multiphase flow view. It divided the tube cross section into three regimes, including liquid-like (LL) core, two-phase-like (TPL) annulus, and vapor-like (VL) film.

The balance of evaporation momentum force and inertia force on vapor-like film near the tube wall is the key to determining the supercritical heat transfer, which can be characterized by the supercritical K number or SBO number. It is proved that SBO number is the key number to determine the overall supercritical heat transfer performance. Specifically, SBO number is a simple criterion to identify the normal heat transfer and heat transfer deterioration. Based on SBO, the supercritical K number introduces a correction factor involving the ratio of density under local bulk temperature to density under local wall temperature. Thus, the supercritical K number has advantages in predicting the local heat transfer performance of supercritical flow. It was confirmed that pseudo-boiling theory is a promising method to analyze supercritical heat transfer in both vertical and

horizontal tube. $^{32-36}$ Here, pseudo-boiling theory involving supercritical K number is used to reveal the influence of tube diameter on local heat transfer of supercritical fluids in horizontal tubes.

In summary, the effect of tube diameter on supercritical heat transfer is an important issue in energy engineering. More investigations were based on experiments, which only obtained temperature at limited locations on the tube wall. The conclusions about the effect of tube diameter on the heat transfer performance of supercritical fluids are also inconsistent in the references. Here, numerical simulations are performed to obtain temperature fields both on the tube and inside the tube. The promising method of pseudo-boiling theory is utilized to obtain supercritical phase distribution in the tube and reveal the effect of tube size on heating sCO₂ in horizontal tubes, including the overall heat transfer performance and non-uniformity in the circumferential direction. This study can not only advance the pseudo-boiling heat transfer theory for supercritical fluids but also offer valuable insights for the secure design of heat exchangers in advanced energy systems.

II. MATHEMATICAL MODEL AND CALCULATION METHOD

A. Physical model

Figure 1 illustrates the physical model of sCO₂ flow in a horizontal tube subjected to uniform heating. The geometric parameters of the tube are consistent with those described in the experimental section of our previous investigation.¹⁰ The horizontal tube is divided into three sections: the inlet adiabatic section, the heating section, and the outlet adiabatic section [see Fig. 1(a)]. The length of the heating section is 3200 mm. The inlet adiabatic section measures 600 mm to ensure the full development of sCO₂ before entering the heating section. Similarly, the outlet adiabatic section is also 600 mm long to ensure a steady flow of sCO₂ at the outlet of the heating section. The flow direction is defined along the z-axis. The inner diameters of the horizontal tube are 8, 10, and 12 mm, with a wall thickness (δ_s) of 2 mm [see Figs. 1(b)-1(d)]. The circumferential direction of the tube is defined as the θ coordinate, where $\theta = 0^{\circ}$ and $\theta = 180^{\circ}$ represent the top and bottom generatrixes of the horizontal tube, respectively. The meshing method is the same as the author's published paper.³⁷

B. The governing equations

The three-dimensional steady-state flow and heat transfer of supercritical CO_2 in a horizontal tube are simulated using ANSYS Fluent 19.2 software. The governing equations, solved by the finite volume method, are as follows:³⁸

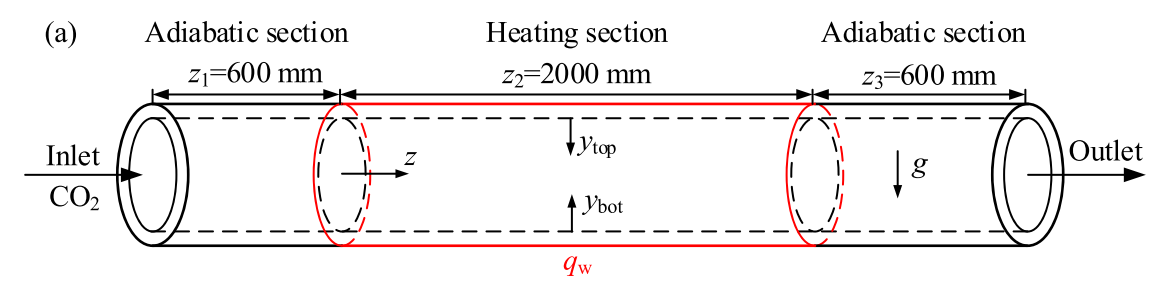
Mass conservation equation

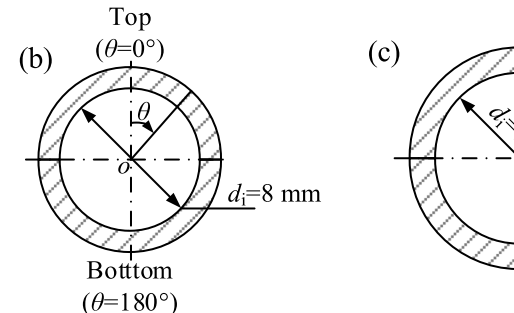
$$\frac{\partial}{\partial x_i}(\rho u_i) = 0. \tag{1}$$

Momentum conservation equation

$$\frac{\partial(\rho u_i u_j)}{\partial x_j} = -\frac{\partial P}{\partial x_i} + \frac{\partial}{\partial x_j} \left[(\mu + \mu_t) \left(\frac{\partial u_i}{\partial x_j} + \frac{\partial u_j}{\partial x_i} - \frac{2}{3} \delta_{ij} \frac{\partial u_k}{\partial x_k} \right) \right] + \rho g_i.$$
(2)

Energy conservation equation





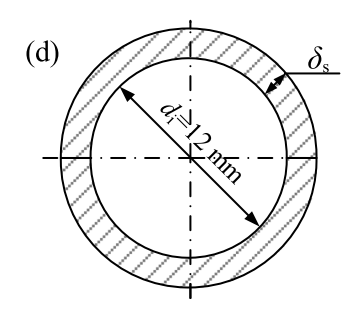


FIG. 1. Physical model.

$$\frac{\partial(\rho u_i c_p T)}{\partial x_i} = \frac{\partial}{\partial x_i} \left[c_p \left(\frac{\mu}{\Pr} + \frac{\mu_t}{\Pr_t} \right) \frac{\partial T}{\partial x_i} \right]. \tag{3}$$

The choice of turbulence model is important for the simulation of supercritical heat transfer. Here, the shear stress transport SST $k-\omega$ turbulence model is used, which outperforms other turbulence models in terms of prediction accuracy reported in the previous research. What is more, this paper investigates the supercritical heat transfer based on pseudo-boiling theory instead of single-phase flow theory modified by buoyancy effects. The prediction of SST $k-\omega$ models is especially accurate near the wall region, which is helpful to obtain the phase distribution details near the wall and reveal the supercritical heat transfer mechanisms in a horizontal tube. The equations of the SST $k-\omega$ turbulence model can be found in ANSYS 19.2 HELP. Turbulent kinetic energy equation

$$\frac{\partial(\rho\mu_i k)}{\partial x_i} = \frac{\partial}{\partial x_j} \left[\left(\mu + \frac{\mu_t}{\sigma_k} \right) \frac{\partial k}{\partial x_j} \right] + G_k - Y_k. \tag{4}$$

Specific dissipation rate equation

$$\frac{\partial(\rho u_i \omega)}{\partial x_i} = \frac{\partial}{\partial x_j} \left[\left(\mu + \frac{\mu_t}{\sigma_{\omega}} \right) \frac{\partial \omega}{\partial x_j} \right] + G_{\omega} - Y_{\omega} + D_{\omega}. \tag{5}$$

In Eqs. (4) and (5), G_k and Y_k terms represent the generation and dissipation of k, G_ω , Y_ω , and Y_ω terms represent the generation, dissipation, and orthogonal divergence of ω , respectively, which are written as follows:

$$G_k = \min(\mu_t S^2, 10\rho \beta^* k\omega), \tag{6}$$

$$Y_k = \rho \beta^* k \omega, \tag{7}$$

$$G_{\omega} = \frac{\alpha_{\infty}}{\alpha_{*}} \left(\frac{\alpha_{0} + \operatorname{Re}_{t}/R_{\omega}}{1 + \operatorname{Re}_{t}/R_{\omega}} \right) \frac{\rho}{\mu_{t}} G_{k}, \tag{8}$$

$$Y_{\omega} = \rho \beta \omega^2, \tag{9}$$

$$D_{\omega} = 2(1 - F1)\rho \frac{1}{\omega \sigma_{\omega 2}} \frac{\partial k}{\partial x_i} \frac{\partial \omega}{\partial x_i}.$$
 (10)

The equations presented above pertain exclusively to the fluid domain. For the solid domain, Fourier's law of thermal conductivity is employed, as expressed in the following equation:

$$\frac{\partial}{\partial x_j} \left(\lambda_s \frac{\partial T}{\partial x_j} \right) + \Phi = 0. \tag{11}$$

Further details regarding the variables and constants in Eqs. (1)–(11) can be found in the comprehensive discussion in Ref. 39.

C. Boundary conditions and solution

The physical properties of CO_2 are derived from REFPROP NIST 9.1.⁴⁰ The inlet of the tube is modeled using a mass flux condition, while the outlet is defined as an outflow boundary. In the heating section of the horizontal tube, a uniform heat flux is applied to the solid outer wall. At the fluid–solid interface, temperature and heat flux are continuous, adhering to a no-slip condition. The governing equations are discretized using the finite volume method. To improve calculation accuracy, a second-order upwind differencing scheme is utilized. The pressure–velocity coupling is resolved using the SIMPLEC algorithm. Convergence is achieved when the residual curves stabilize and the monitored outlet temperature approaches a steady state. The relative residuals for the mass and momentum transport equations are set to 10^{-3} , while the relative residual for the energy transport equation is set to 10^{-9} .

In this paper, the selection of parameter ranges considers the practical operating conditions of the evaporator in the sCO2 heat pump⁴¹ and the boiler in the sCO₂ power generation system.³² The inlet temperature is normal atmospheric temperature (293 K). The inlet pressure is 10-20 MPa, which is larger than the critical pressure of CO₂ (7.377 MPa). The ranges of mass flux and heat flux are 700-1300 kg/m² s and 66.7–300 kW/m², respectively. Specifically, this paper focuses on the influence of tube diameter on heat transfer performance. The heat transfer performance of CO2 is worse than that of water steam. Thus, it is a wise choice to use a small tube to increase the heat transfer area in a finite space. Of course, reducing the pipe diameter can also cause a large pressure drop. Fortunately, module design of sCO₂ heat exchangers can control flow resistance to the same level of steam heat exchangers based on partial flow strategy, which changes long pipelines in series to short pipelines in parallel. 42 Finally, the range of inner tube diameter is selected as 8-12 mm according to the related investigations and engineering application. 6,10,43-45 It is noted that the

tube size range seems narrow. However, the flow area changes more than two times and the influence of tube size is remarkable, which will be verified in Sec. III.

D. Validation of grid independence and model accuracy

To guarantee the authenticity and correctness of the simulated outcomes, a grid independence analysis is conducted (see Fig. 2). Figures 2(a) and 2(b) illustrate the variation of the inner wall temperature $T_{\rm wi}$ with bulk enthalpy $i_{\rm b}$ under four grid conditions. The $T_{\rm wi}$ rises gradually along the flow direction, performing normal heat transfer (NHT) [see Fig. 2(a)], and the $T_{\rm wi}$ along the flow direction exhibits a noticeable peak, inducing heat transfer deterioration (HTD) [see Fig. 2(b)]. The results show that computed values of inner wall temperature tend to be stable with increasing grid number. The average error of the inner wall temperature values calculated with grid numbers of

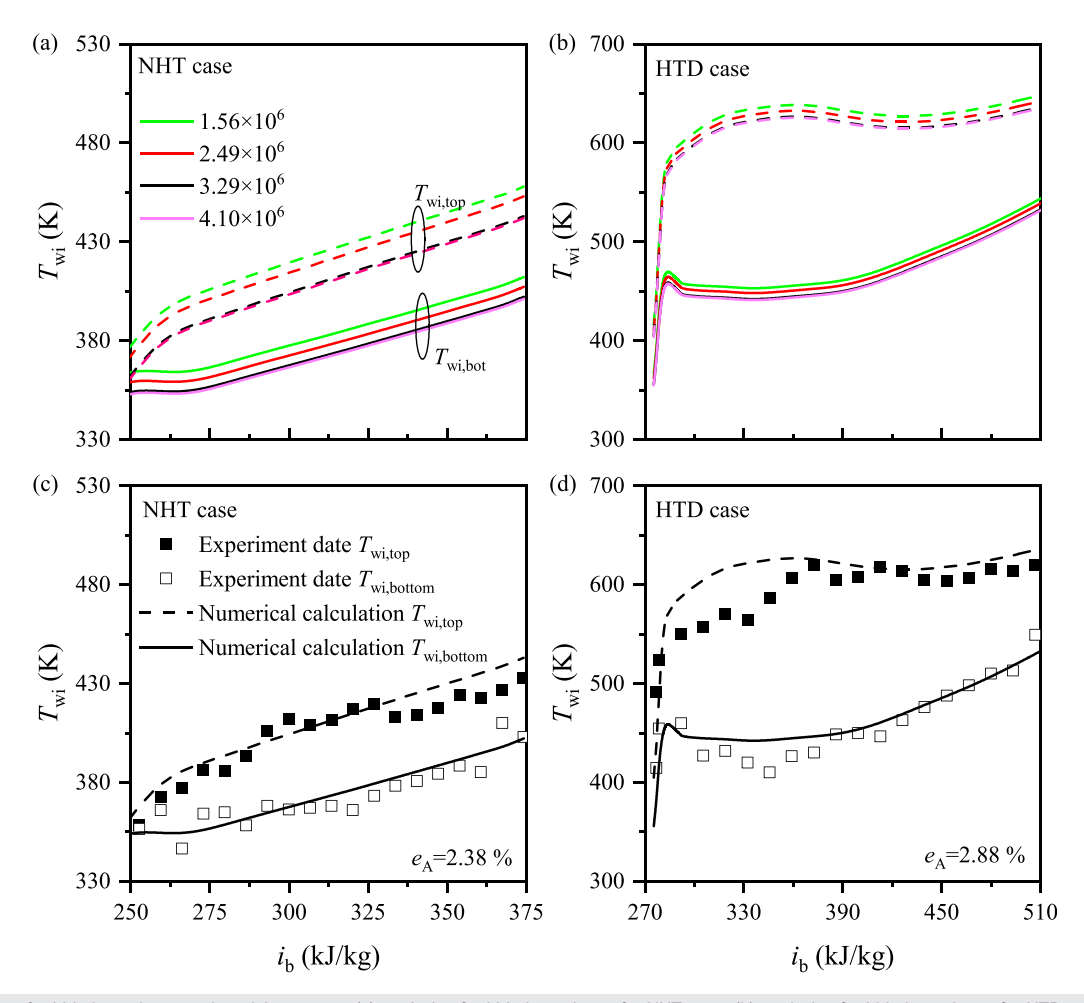


FIG. 2. Validation of grid independence and model accuracy: (a) analysis of grid independence for NHT case; (b) analysis of grid independence for HTD case; (c) validation of numerical result with experimental data for NHT case; and (d) validation of numerical result with experimental data for HTD case. Not that the experiment data are from Ref. 10. The NHT case is $d=12 \,\mathrm{mm},\ P=20.1 \,\mathrm{MPa},\ G=1008.5 \,\mathrm{kg/m^2} \,\mathrm{s},\ q_\mathrm{w}=207.1 \,\mathrm{kW/m^2},\$ and the HTD case is $d=12 \,\mathrm{mm},\ P=8.1 \,\mathrm{MPa},\ G=773.9 \,\mathrm{kg/m^2} \,\mathrm{s},\$ and $q_\mathrm{w}=312.6 \,\mathrm{kW/m^2}.$

 3.29×10^6 and 4.10×10^6 is only 0.24% and 0.19% for the NHT and HTD case, respectively. Therefore, to balance calculation time and accuracy, the grid number of 3.29×10^6 is selected for the simulation.

The numerical simulation is validated using experimental data from Ref. 10. The heating horizontal tube's geometric parameters are the same in the experiment and the simulation. Figures 2(c) and 2(d) illustrate the comparison of the numerical simulation results of NHT conditions and HTD conditions with the experimental data. The graphic demonstrates that the inner wall temperature ($T_{\rm wi}$) determined by simulation varies with the bulk enthalpy, in accordance with the experimental results. The formula for calculating the average error between the simulated values and the experimental data are as follows:

$$e_{\rm A} = \frac{1}{n} \sum_{i=1}^{n} e_i \times 100\%,$$
 (12)

where e_i represents the error for a single data point, $e_i = (T_{\text{wi, pre}} - T_{\text{wi, exp}})/T_{\text{wi, exp}}$. As a result, the average error is only 2.38% and 2.88% [see Figs. 2(c) and 2(d)]. Therefore, the numerical model employed in this study is both feasible and reliable.

III. RESULTS AND DISCUSSION

A. Heat transfer performance of sCO₂ in horizontal tube

Heat transfer performance of forced convection is determined by both the inner wall temperature T_{wi} and the bulk temperature of fluids T_{b} . The heat transfer coefficient h is defined as follows:

$$h = \frac{q_{\text{wi}}}{T_{\text{wi}} - T_{\text{b}}},\tag{13}$$

where the heat flux on the inner wall of the horizontal tube is

$$q_{\rm wi} = q_{\rm w} \left(\frac{d_{\rm out}}{d_{\rm in}} \right). \tag{14}$$

It notes that the heat transfer performances in the circumferential direction are non-uniform due to different wall temperatures. Specifically, $h_{\rm top}$ and $h_{\rm bot}$ are calculated by Eq. (13) using $T_{\rm wi}$ at the top generatrix and bottom generatrix, respectively.

Figure 3 depicts the distribution of temperature and heat transfer coefficient h with bulk enthalpy i_b for a 12 mm diameter tube at P = 10 MPa and $G = 700 \text{ kg/m}^2 \text{ s}$. Under the low heat flux condition of $q_{\rm wi} = 66.7 \,\rm kW/m^2$, the inner wall temperature $T_{\rm wi}$ rises gradually with i_b , performing normal heat transfer NHT [see Fig. 3(a)]. At a high heat flux of $q_{wi} = 225 \text{ kW/m}^2$, the variation curves of T_{wi} with i_b show a significant peak, behaving heat transfer deterioration HTD [see Fig. 3(b)]. To characterize the overshoot temperature of such a peak quantitatively, mark the highest wall temperature point A at the peak and the lowest wall temperature point B at the downstream of the peak. The wall temperature difference between points A and B is defined as overshoot temperature, which achieves 13.3 and 20.9 K at top and bottom generatrixes, respectively [see Fig. 3(b)]. For both NHT and HTD cases in a horizontal tube, the $T_{wi, top}$ is consistently higher than that of $T_{wi, top}$ bot. In conclusion, HTD in horizontal tubes creates not only a wall temperature overshoot in the flow direction but also substantial wall temperature non-uniformity in the circumferential direction.

For the NHT case under $q_{wi} = 66.7 \text{ kW/m}^2$, both the heat transfer coefficient at top generatrix h_{top} and bottom generatrix h_{bot} rise

continuously with the i_b [see Fig. 3(c)]. From the perspective of traditional single-phase flow theory, the Reynolds number Re and Prandtl number Pr are the fundamental dimensionless parameters governing the heat transfer. Usually, the larger Re and Pr indicate the better heat transfer performance. Re and Pr are defined as follows:

$$Re = \frac{Gd}{\mu},\tag{15}$$

$$Pr = \frac{c_{\rm p}\mu}{\lambda},\tag{16}$$

where $c_{\rm p}$ and μ are specific heat capacity and viscosity, respectively. Under heating condition, $T_{\rm b}$ of supercritical fluids in the tube always rises, reducing dynamic viscosity μ and rising Reynolds number Re in the flow direction [see Fig. 3(e)]. In addition, Pr also increases in the flow direction due to rising $T_{\rm b}$ [see Fig. 3(f)]. Thus, it seems reasonable that the heat transfer coefficient rises continuously with the $i_{\rm b}$ in Fig. 3(c).

For the HTD case under $q_{\rm wi} = 225\,{\rm kW/m^2}$, the $h_{\rm top}$ first decreases sharply and then rises slowly along the flow direction. The $h_{\rm bot}$ decreases and then increases, when $i_{\rm b} > 392.1\,{\rm kJ/kg/K}$, the $h_{\rm bot}$ shows a decreasing trend again [see Fig. 3(d)]. However, both Re and Pr increase at the inlet of the tube [see Figs. 3(g) and 3(h)], which fails to explain the heat transfer deterioration at the inlet of the tube. Thus, there must be some other factors to influence the supercritical heat transfer, which attribute the sensitive changes of physical property for single-phase flow theory. Unfortunately, such treatment of single-phase flow theory is complex and inconsistent in previous investigations.

Instead, pseudo-boiling theory is utilized to elucidate the heat transfer behavior of sCO₂ in horizontal tubes in the following discussions. The temperature distributions within the tubes were obtained and converted into phase distributions based on pseudo-boiling theory (see Fig. 4). The supercritical fluid in tube cross section is divided into three regimes, including liquid-like (LL), two-phase-like (TPL), and vapor-like (VL) according to the supercritical heat transfer model proposed by Wang *et al.*²⁷ The change from LL to TPL occurs at the T^- temperature, assuming that the change from TPL to VL occurs at T^+ temperature, where T^- and T^+ are determined by the thermodynamic method. Of For easy analysis, the thickness of the vapor-like film δ is defined as the vertical distance from the wall to T^+ (see Fig. 4).

Figures 4(a) and 4(c) illustrate the phase distribution of sCO₂ within the tube for NHT case. The proportion of high specific heat liquid-like working fluids inside the tube is relatively high, which enhances heat transfer between the working fluid and the tube wall. This explains the increasing trend of the HTC observed with the i_b in Fig. 3(c). Figures 4(b) and 4(d) show the phase distribution of the sCO₂ inside the tube for HTD case. As seen in Fig. 4(b), the top of the tube is predominantly occupied by a significant amount of vapor-like sCO₂, with an increased growth rate of the vapor-like film. As a result, the h_{top} first decreases sharply with increasing i_{b} . The heat transfer performance of the tube is recovered at $i_{\rm b} > 344.5\,{\rm kJ/kg/K}$ with the decrease in the growth rate of the vapor-like film and the larger in the thermal conductivity in the near-wall region [see Fig. 3(d)]. As shown in Fig. 4(d), the vapor-like film at the bottom of the tube initially expands and then decreases. This behavior explains the trend observed for the heat transfer coefficient h_{bot} concerning i_{b} in Fig. 3(d), where $h_{\rm bot}$ decreases initially before increasing. When $i_{\rm b} > 392.1\,{\rm kJ/kg/K}$, the vapor-like film's thickness thickens significantly, severely hindering

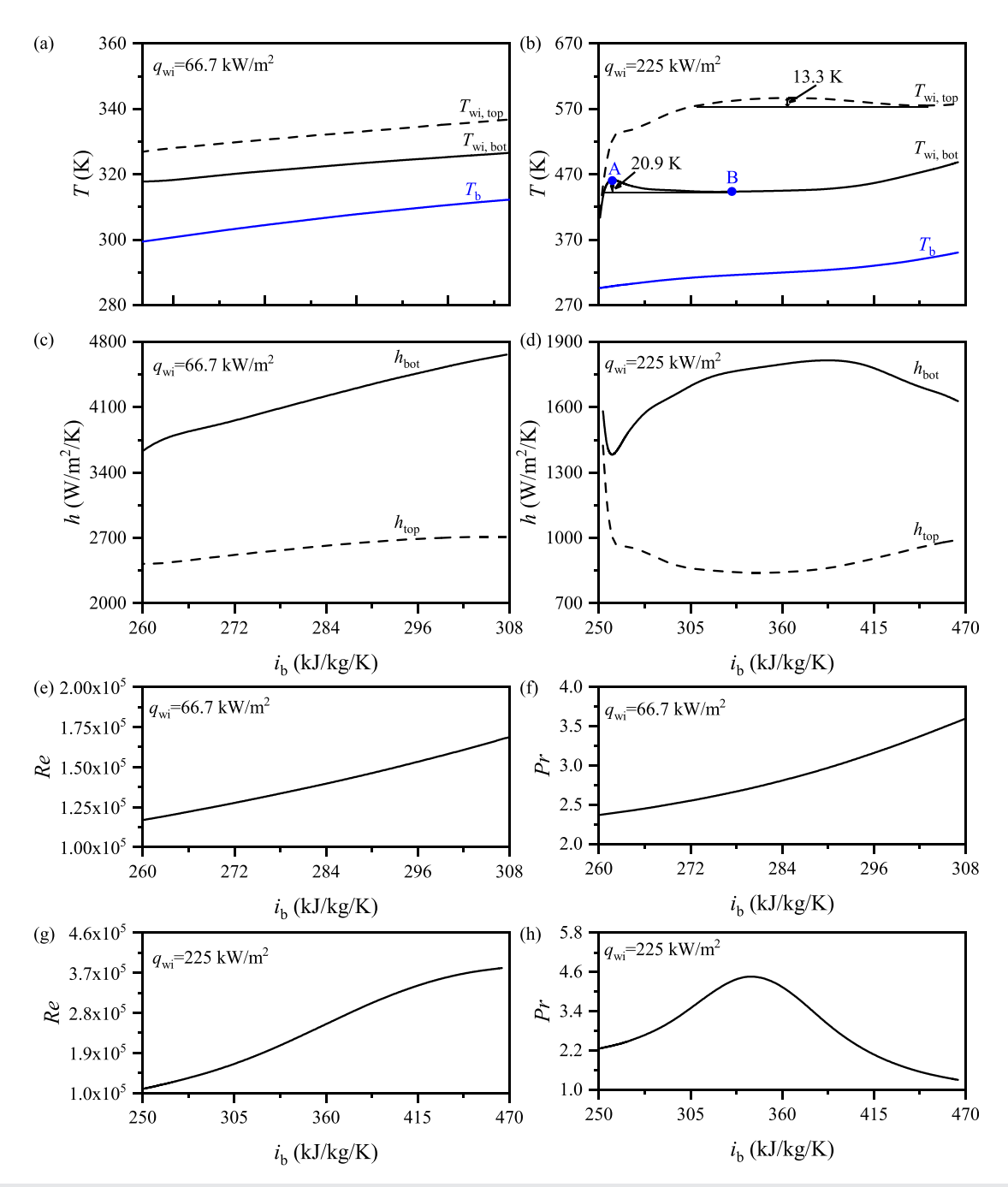


FIG. 3. Variation of the temperature, heat transfer coefficient, Reynolds number Re and Prandtl number Pr with the bulk enthalpy i_b under different heat flux $(d_{in} = 12 \text{ mm}, P = 10 \text{ MPa}, \text{ and } G = 700 \text{ kg/m}^2\text{s})$: (a), (c), (e), and (f) are normal heat transfer NHT case under heat flux of 66.7 kW/m²; (b), (d), (g), and (h) are heat transfer deterioration HTD case under heat flux of 225.0 kW/m².

the heat exchange between the fluid and the wall in the tube, and thus $h_{
m bot}$ again shows a decreasing trend.

Compared to vertical tubes, the flow in horizontal tubes is more complex. In cases of HTD, the risk of tube rupture is not only due to overheating but also to stress-induced failures caused by uneven temperature distribution. Therefore, it is crucial to study the variations in temperature differences between the top and bottom of the tube. Figure 5(a) illustrates the variation in the temperature difference ΔT between the top and bottom generatrix as a function of the $i_{\rm b}$ curve. The ΔT initially increases and then decreases.

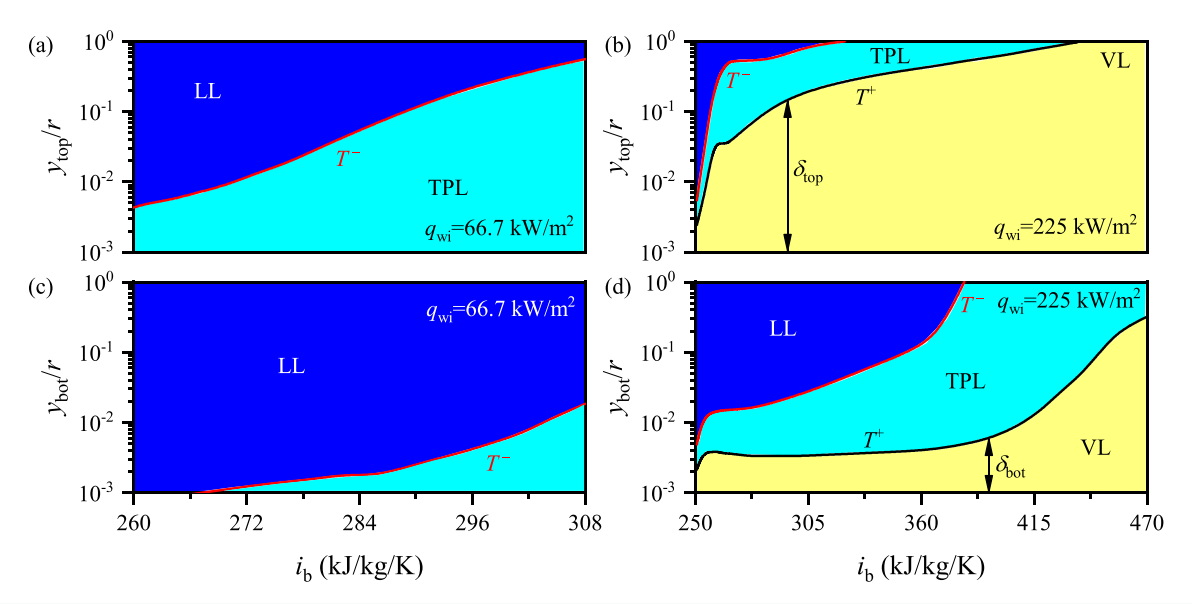


FIG. 4. Variations of phase distribution and with the bulk enthalpy i_b at the top and bottom of the horizontal tube (P = 10 MPa, $G = 700 \text{ kg/m}^2 \text{s}$): (a) and (c) are NHT case; and (b) and (d) are HTD case.

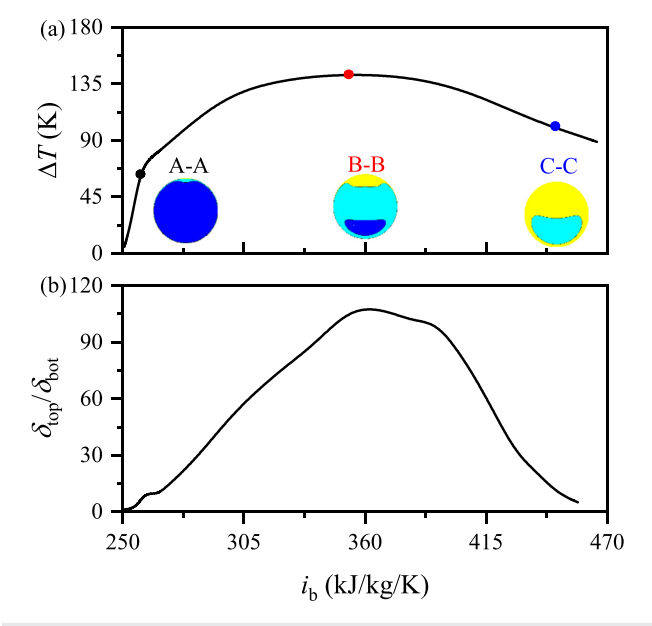


FIG. 5. Variation of the temperature difference between the top and bottom generatrix ΔT and vapor-like film thickness ratio $\delta_{\text{top}}/\delta_{\text{bot}}$ with bulk enthalpy i_{b} for HTD case (P=10 MPa, G=700 kg/m²s, and $q_{\text{wi}}=225$ kW/m²/s).

Phase distributions were obtained for the three characteristic cross sections: A-A, B-B, and C-C. The cross section A-A is predominantly filled with liquid-like sCO₂. Along the flow direction, a stratified distribution of vapor-like and liquid-like states develops in the cross section at location B-B. The top of the tube is covered by a vapor-like film, which impedes heat exchange between the fluid inside the tube and the wall. Meanwhile, at the bottom of the tube, the liquid-like state of sCO₂, with its high specific heat, continues to exchange heat with

the surrounding wall materials. Consequently, the ΔT gradually rises from cross section A-A to cross section B-B.

During the transition from location B-B to location C-C, the temperature inside the tube rises gradually. The stratification between the vapor-like and liquid-like phases diminishes, and the liquid-like sCO₂ phase disappears. At this point, the tube's top and bottom are enveloped by a vapor-like film, which further impedes heat transfer between the fluid and the tube wall. As a result, the ΔT decreases progressively from section B-B to section C-C.

Figure 5(b) demonstrates the variation of the vapor-like film thickness ratio $\delta_{\rm top}/\delta_{\rm bot}$ with the $i_{\rm b}$ for the top and bottom generatrix of the tube. An increase in the $\delta_{\rm top}/\delta_{\rm bot}$ ratio indicates that the thermal resistance at the top of the tube is higher, while the heat transfer resistance at the bottom is relatively low. This disparity results in inefficient heat exchange at the top of the tube, while the heat exchange at the bottom is more effective. Therefore, as $\delta_{\rm top}/\delta_{\rm bot}$ increases, ΔT rises; conversely, as $\delta_{\rm top}/\delta_{\rm bot}$ decreases, ΔT decreases.

B. Effect of tube diameter on HTC

Figures 3–5 indicate that the vapor-like film thickness is the primary parameter determining the supercritical heat transfer performance. According to pseudo-boiling theory, the vapor-like film thickness can be characterized by the supercritical K number proposed by Zhu *et al.*²⁸ Specifically, the larger the supercritical K value, the thicker the vapor-like film. Physically, the supercritical K number denotes the competition between evaporative momentum forces and inertial forces on vapor-like film, which is calculated as follows:²⁸

$$K = \left(\frac{q_{\rm w}}{G\Delta i}\right)^2 \frac{\rho_{T^-}}{\rho_{T_{\rm w}}},\tag{17}$$

where ρ_{T^-} and ρ_{T_w} are the densities of the fluid at T^- and T_w , respectively and Δi is the pseudo-boiling enthalpy²⁷

$$\Delta i = \int_{T^{-}}^{T^{+}} c_{\mathbf{p}} dT = i(T^{+}) - i(T^{-}).$$
 (18)

It notes that the difference of $T_{\rm w}$ at the top generatrix and bottom generatrix can result in supercritical $K_{\rm top}$ and $K_{\rm bot}$ numbers, respectively.

In addition, the heat transfer performance is also affected by the physical properties of vapor-like film. Thus, Yan *et al.*⁴⁶ and Zhang *et al.*⁴⁷ proposed the thermal conductivity resistance to consider both thickness and physical properties of vapor-like film, which is calculated as follows:

$$R_{\rm VL} = \int_0^\delta (1/\lambda_{\rm VL}) dy,\tag{19}$$

where y is the vertical distance from the wall, δ is the thickness of the vapor-like film defined as the vertical distance from the wall to T^+ , and $\lambda_{\rm VL}$ is the average heat conduction in the vapor-like film, respectively. Here, the thermal conductivity resistances $R_{\rm VL,\ top}$ and $R_{\rm VL,\ bot}$ at the top generatrix and bottom generatrix are used to reveal the effect of tube diameter on HTC.

Figure 6 shows the tube diameter effect on the heat exchange at the top of the horizontal tube. As the tube diameter increases, K_{top} rises

[see Fig. 6(a)], suggesting that a larger tube diameter enhances the evaporation momentum force, which overcomes the inertial force and leads to the formation of a thicker vapor-like film. This expanded film thickness results in higher thermal resistance $R_{\rm VL}$ [see Fig. 6(b)]. Consequently, heat transfer between the fluid inside the tube and the top wall is hindered, causing the $T_{\rm wi,\ top}$ to rise as the tube diameter increases [see Fig. 6(c)], while the $h_{\rm top}$ decreases [see Fig. 6(d)].

Figure 7 illustrates the impact of tube diameter on heat transfer at the bottom of the horizontal tube. The results show that $K_{\rm bot}$ is relatively maximum when the tube diameter $d_{\rm in}=12$ mm, while it is relatively minimum when $d_{\rm in}=10$ mm [see Fig. 7(a)]. The $K_{\rm bot}$ exhibits a nonlinear relationship with increasing tube diameter. As the evaporative momentum force at the tube's bottom enhances, its ability to overcome the inertial force also strengthens, resulting in the minimum $R_{\rm VL, bot}$ at $d_{\rm in}=10$ mm [see Fig. 7(b)]. This explains the variation pattern of the inner wall temperature $T_{\rm wi, bot}$ of the bottom generatrix with the $i_{\rm b}$, as shown in Fig. 7(c). Since the $R_{\rm VL, bot}$ reaches its maximum at $d_{\rm in}=12$ mm, this significantly impedes heat exchange between the fluid inside the tube and the tube's top wall, resulting in a minimum HTC under these conditions [see Fig. 7(d)]. The effect of tube diameter is most pronounced at the top of the tube, while at the

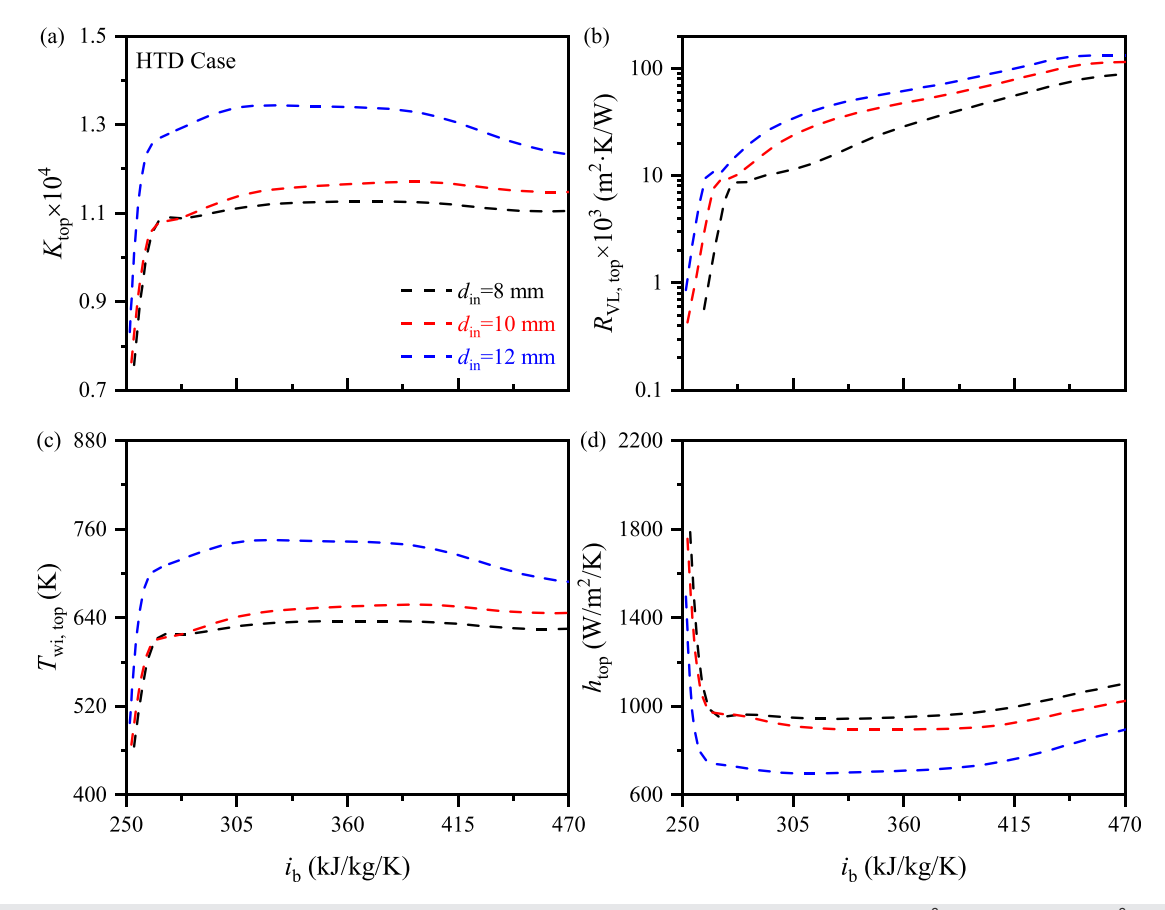


FIG. 6. Effect of tube diameter on heat transfer performance at the top generatrix of horizontal tube (P = 10 MPa, $G = 700 \text{ kg/m}^2 \text{s}$, and $q_{wi} = 300 \text{ kW/m}^2$): variation of (a) supercritical K_{top} , (b) vapor-like film thermal resistance $R_{\text{VL}, \text{top}}$, (c) inner wall temperature $T_{\text{wi}, \text{top}}$, and (d) heat transfer coefficient h_{top} with bulk enthalpy i_{b} under different tube diameters.

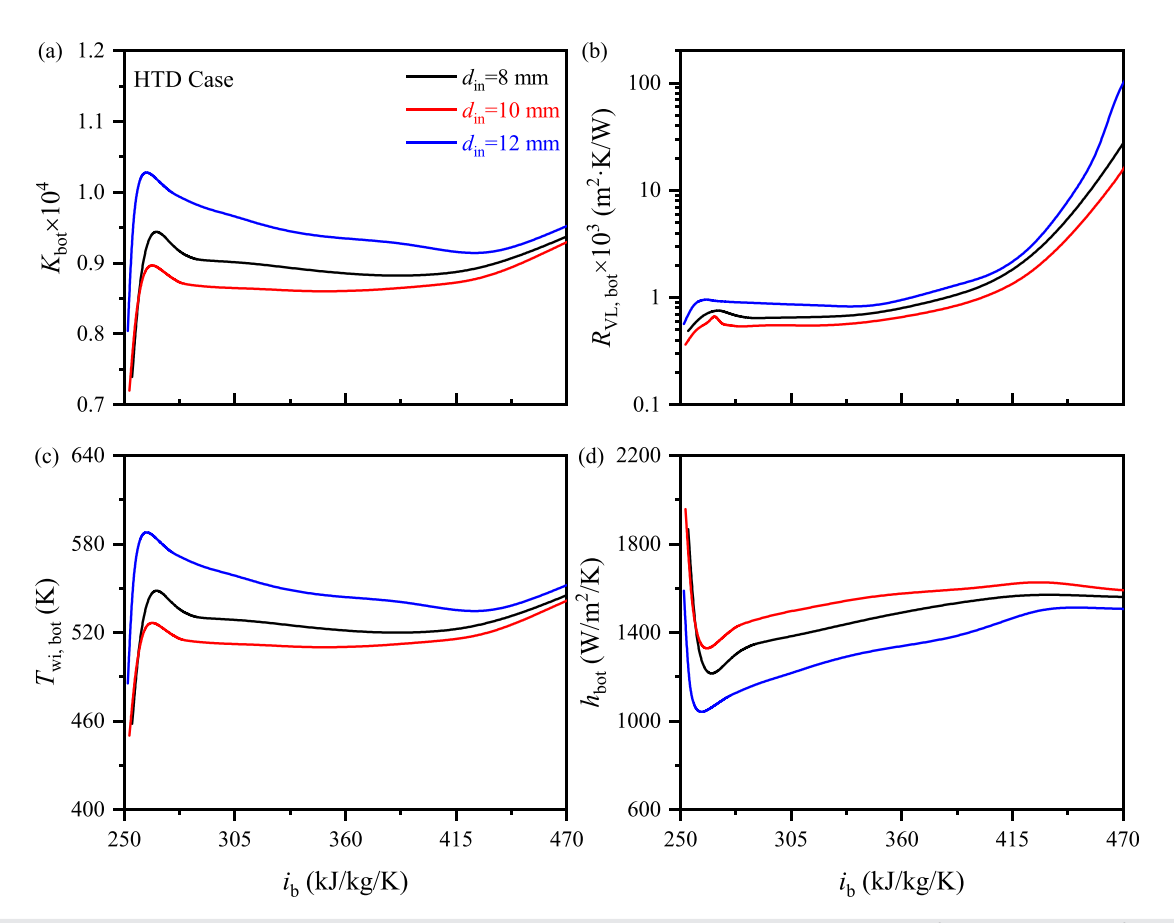


FIG. 7. Effect of tube diameter on heat transfer performance at the bottom generatrix of horizontal tube (P = 10 MPa, $G = 700 \text{ kg/m}^2 \text{s}$, and $q_{wi} = 300 \text{ kW/m}^2$): variation of (a) supercritical K_{bot} , (b) vapor-like film thermal resistance $R_{\text{VL, bot}}$, (c) inner wall temperature $T_{\text{wi, bot}}$, and (d) heat transfer coefficient h_{bot} with bulk enthalpy i_{b} under different tube diameters

bottom, the effect exhibits a nonlinear relationship. This was also observed in the experimental study by Cheng *et al.*¹⁰

C. Effect of tube diameter on ΔT

The analysis of temperature differences between the top and bottom generatrix is crucial for ensuring the safe and stable operation of solar power cycles, as well as for the design of heat exchange equipment. Figure 8 shows the effect of tube diameter on the difference in heat transfer under HTD conditions. The $K_{\rm top}/K_{\rm bot}$ ratio rises substantially with increasing tube diameter [see Fig. 8(a)], indicating that the larger tube diameter causes a notable difference in evaporative momentum forces at the top and bottom of the tube. Simultaneously, the ratio $\delta_{\rm top}/\delta_{\rm bot}$ grows with increasing tube diameter [see Fig. 8(b)]. Thus, ΔT rises with increasing tube diameter [see Fig. 8(c)].

The cross-sectional phase distribution of sCO₂ was obtained for different tube diameters at the bulk enthalpy $i_b = 368.9 \,\mathrm{kJ/kg}$, as shown in Fig. 9. It is evident that the thickness of the vapor-like film at the top of the tube exceeds that at the bottom, with a distinct stratification effect between the vapor-like and liquid-like phases across the tube's cross section. This phenomenon explains why ΔT reaches its maximum value in this region.

The supercritical K number, vapor-like film thermal conductivity thermal resistance R_{VI} , inner wall temperature T_{wi} , and circumferential variation of heat transfer coefficient h were obtained as shown in Figs. 10(a)-10(d). The supercritical K number decreases with increasing angle from the top $(\theta = 0^{\circ})$ to the bottom $(\theta = 180^{\circ})$ of the tube [see Fig. 10(a)]. This reduction causes a corresponding decrease in $R_{\rm VL}$ and T_{wi} in the circumferential direction [see Figs. 10(b) and 10(c)], which subsequently leads to a rise in h [see Fig. 10(d)]. The effect of tube diameters is similar between the flow direction and the circumferential direction. When $\theta = 0^{\circ}$, the supercritical K becomes larger with the increase in the tube diameter. When $\theta = 180^{\circ}$, the supercritical K changes nonlinearly. In the circumferential direction, the variation trends of supercritical K, R_{VL} , and T_{wi} are the same. This explanation accounts for the circumferential variation of h [see Fig. 10(d)]. This suggests that at the top of the tube, heat transfer performance improves with smaller tube diameters, whereas at the bottom of the tube, the heat transfer effect exhibits a nonlinear variation with respect to the tube diameter.

In practical engineering applications, greater emphasis is placed on the variation in total heat transfer. Consequently, the effect of tube diameter on overall heat transfer is determined (see Fig. 11). The $T_{\rm wi,\,ave}$ and $h_{\rm ave}$ are the circumferentially averaged internal wall

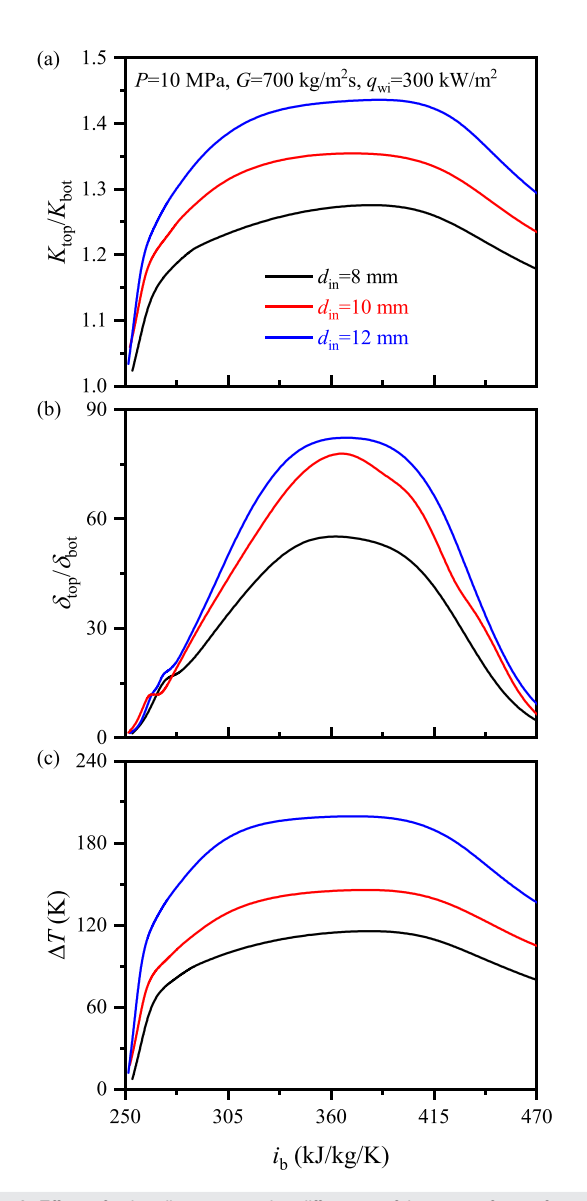


FIG. 8. Effect of tube diameter on the difference of heat transfer performance between top and bottom generatrix ($P=10\,\mathrm{MPa}$, $G=700\,\mathrm{kg/m^2\,s}$, and $q_\mathrm{wi}=300\,\mathrm{kW/m^2}$): variation of (a) supercritical $K_\mathrm{top}/K_\mathrm{bot}$, (b) vapor-like film thickness ratio $\delta_\mathrm{top}/\delta_\mathrm{bot}$, and (c) temperature difference between the top and bottom generatrix ΔT with bulk enthalpy i_b under different tube diameters.

temperature and average heat transfer coefficient, respectively. The value of $K_{\rm ave}$ decreases as the tube diameter decreases [see Fig. 11(a)], suggesting that, at smaller diameters, inertial forces dominate over evaporative momentum forces. This leads to the formation of a thinner vapor-like film, which results in reduced $R_{\rm VL}$, ave as the tube diameter decreases [see Fig. 11(b)], which is favorable for the heat exchange between the fluid inside the tube and the wall of the tube, so that the inner wall temperature $T_{\rm wi,\ ave}$ decreases with reducing tube diameter [see Fig. 11(c)], and $h_{\rm ave}$ enhanced significantly with decreasing tube diameter [see Fig. 11(d)]. Therefore, it is preferable to choose a small tube diameter in the design of the heat exchanger.

D. Influence of pressure

The influence of tube diameter on heat transfer performance at $P = 10 \,\mathrm{MPa}$ is analyzed in Figs. 6–11. Additionally, the operating parameters are expanded to 20 MPa to improve the study's comprehensiveness. According to pseudo-boiling theory, supercritical heat transfer performance is influenced by three dimensionless numbers, including Re, Pr, and supercritical K number. 28 Figure 12 shows the change of heat transfer coefficients and the above dimensionless numbers in the flow direction under different pressures. It is found that heat transfer coefficients are larger under larger pressure [see Fig. 12(a)]. However, Pr is smaller due to reducing specific heat capacity and Re is also smaller due to rising dynamic viscosity under higher pressure [see Figs. 12(b) and 12(c)]. On the other hand, the previous investigation confirmed that rising pressure reduces the thickness of the vapor-like film.⁴⁵ Thus, the smaller supercritical K number is the main reason to determine the larger heat transfer coefficients under higher pressure [see Fig. 12(d)], which overwhelms the effects of Re and Pr. Accordingly, the influence of tube diameter on heat transfer at various pressures is mainly discussed with supercritical K number as follows.

Figure 13 illustrates the impact of tube diameter on heat transfer at various pressures. As shown in the figure, at pressures of 10, 15, and 20 MPa, the influence of tube diameter on $T_{\rm wi}$ and K follows the same trend observed at lower pressures. However, when $i_{\rm b}>i_{\rm pc}$, the effect of tube diameter on the $T_{\rm wi}$, bot diminishes as pressure improves. This is primarily due to the rising proportion of the vapor-like phase flow in the tube's cross section when $i_{\rm b}>i_{\rm pc}$ which weakens the stratification of the flow.

Figure 14 shows the effect of tube diameter on ΔT at different pressures. The ΔT rises with increasing tube diameter, which is mainly due to the change in the supercritical $K_{\rm top}/K_{\rm bot}$ ratio. For $d_{\rm in}=12$ mm, the $\Delta T_{\rm max}$ decreases from 199.7 K to 160.4 K when the pressure is improved from 10 to 20 MPa, a decrease in 19.6%. In contrast, for $d_{\rm in}=8$ mm, $\Delta T_{\rm max}$ decreased by 8.3%. This indicates that the increase in tube diameter has a relatively small effect on the $\Delta T_{\rm max}$ value.

E. Influence of mass flux

The above discussion is mainly under a fixed mass flux $G = 700 \, \mathrm{kg/m^2} \, \mathrm{s}$. Here, the influence of mass flux in the range of 700–1300 $\, \mathrm{kg/m^2} \, \mathrm{s}$ is investigated. Figure 15 shows the change of heat transfer coefficients and the related dimensionless numbers in the flow direction under different mass fluxes. It is found that increasing mass flux G behaves ignorable influence on Pr, but increases Re and reduces supercritical K number significantly. Thus, better supercritical heat transfer performances are achieved under larger mass flux by rising inertial force and reducing vapor-like film thickness. According to Eqs. (15) and (17), Re is proportional to G and supercritical K number is inversely proportional to G^2 . Thus, the change of K vs G behaves more significant.

Figure 16 illustrates the impact of tube diameter on heat transfer at various mass fluxes. The convective heat transfer is enhanced, leading to a more effective reduction in wall temperature. This increased mass flux also contributes to significant mitigation of wall temperature overshoot, thereby inhibiting the occurrence of HTD [see Fig. 16(a)]. According to Eq. (17), increasing the mass flux amplifies the inertial force, so supercritical *K* decreases with increasing mass flux

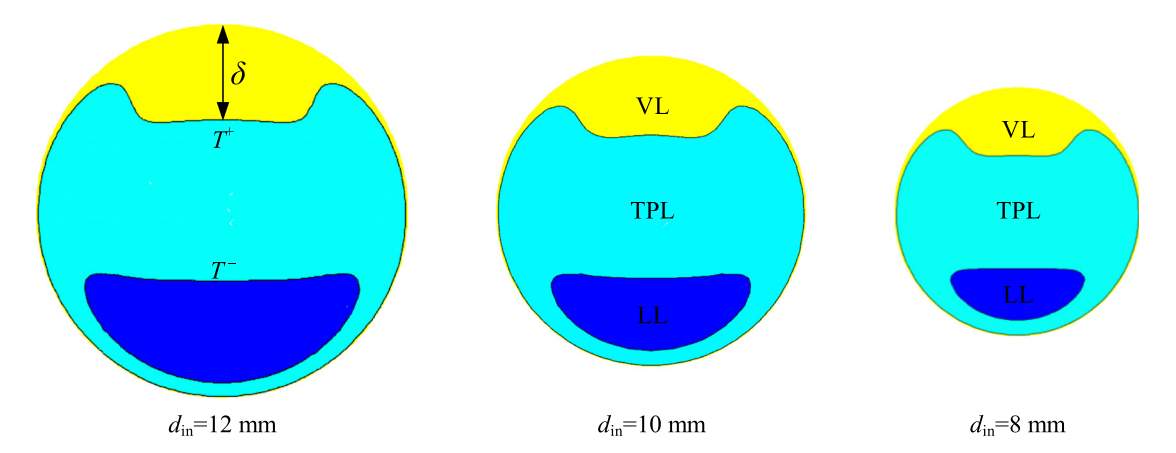


FIG. 9. Phase distribution of heating sCO₂ in horizontal tubes with different diameters (P = 10 MPa, $G = 700 \text{ kg/m}^2 \text{s}$, $q_{wi} = 300 \text{ kW/m}^2$, and $i_b = 368.9 \text{ kJ/kg}$).

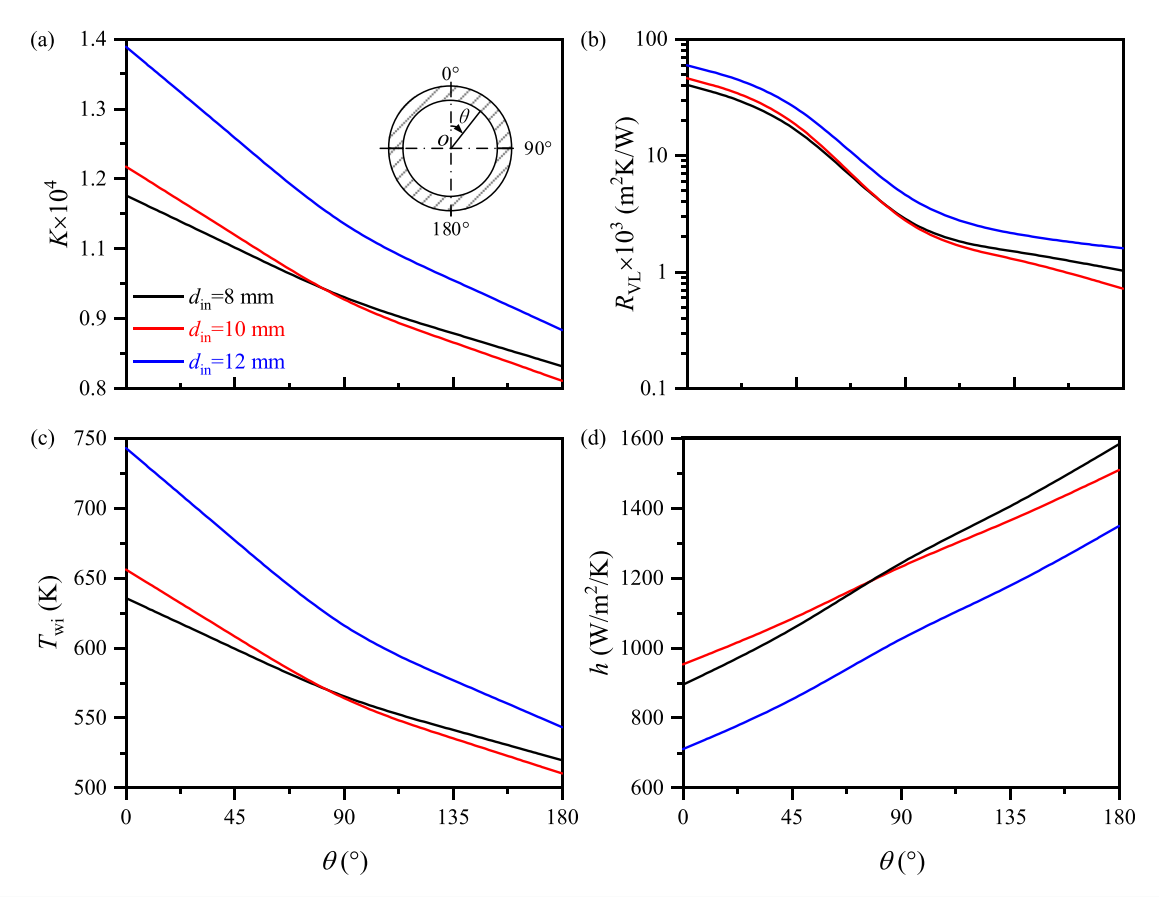


FIG. 10. Effect of tube diameter on heat transfer performance in circumferential direction (P = 10 MPa, $G = 700 \text{ kg/m}^2 \text{s}$, $q_{wi} = 300 \text{ kW/m}^2$, and $i_b = 368.9 \text{ kJ/kg}$): variation of (a) supercritical K number, (b) thermal resistance of vapor-like film R_{VL} , (c) inner wall temperature T_{wi} , and (d) heat transfer coefficient h with polar angle θ .

[see Fig. 16(b)], thereby reducing the thickness of the vapor-like film and enhancing heat transfer performance.

Figure 17 illustrates the effect of tube diameter on ΔT and $K_{\text{top}}/K_{\text{bot}}$ at different mass fluxes. The ΔT initially rises and then decreases along

the flow direction, which is attributed to the supercritical $K_{\rm top}/K_{\rm bot}$ values variation. At high mass flux, the $\Delta T_{\rm max}$ decreases significantly. For $d_{\rm in} = 12$ mm, the $\Delta T_{\rm max}$ decreases from 199.7 to 112.1 K when the mass flux is raised from 700 to 1300 kg/m²s, a decrease in 43.9% is

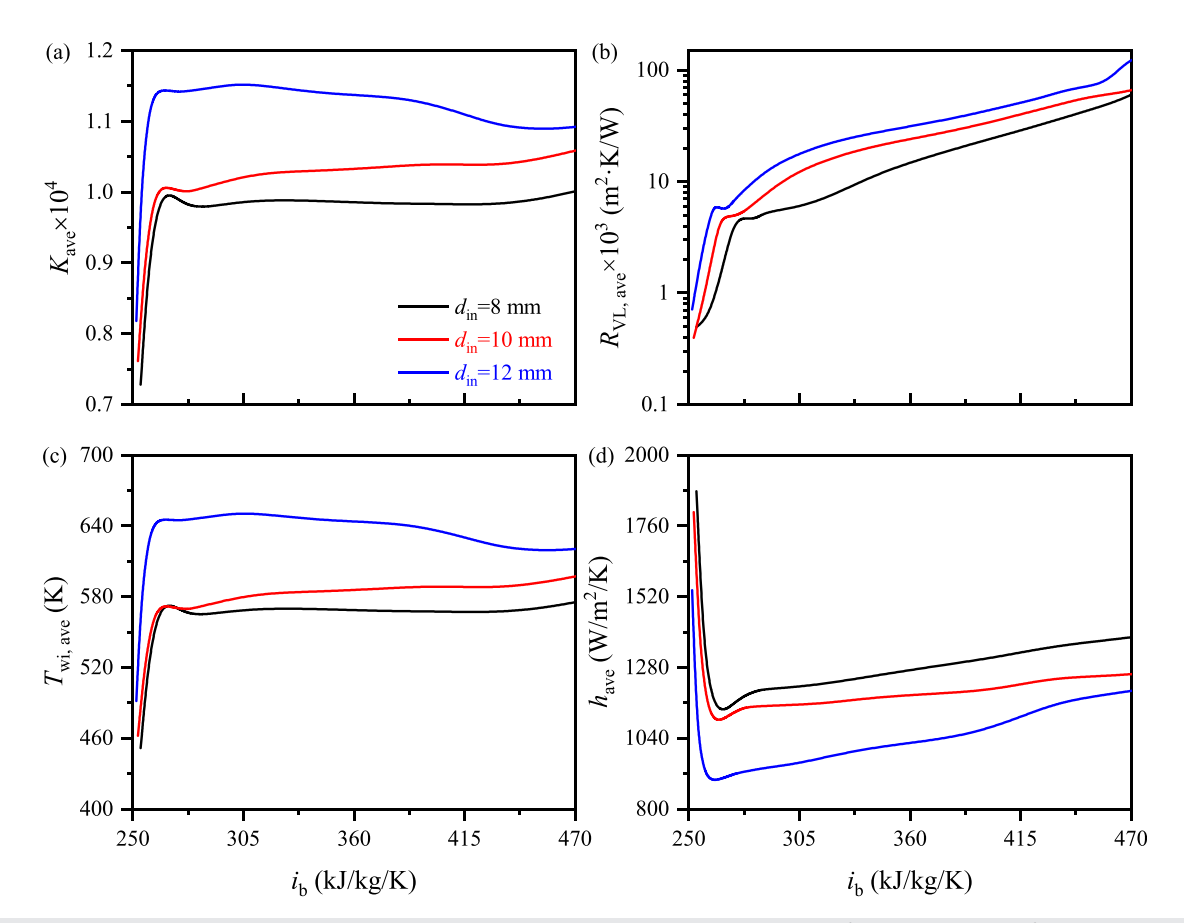


FIG. 11. Effect of tube diameter on the overall heat transfer performance in horizontal tube ($P=10\,\mathrm{MPa}$, $G=700\,\mathrm{kg/m^2}$ s, and $q_\mathrm{wi}=300\,\mathrm{kW/m^2}$): variation of (a) supercritical K_ave , (b) thermal resistance of vapor-like film R_VL , ave, (c) inner wall temperature T_wi , ave, and (d) heat transfer coefficient h_ave with bulk enthalpy i_b under different tube diameters

observed. In contrast, for $d_{\rm in}=8$ mm, $\Delta T_{\rm max}$ decreased by 44.9%. The increase in mass flux leads to a larger inertial force of the fluid within the tube, which reduces the flow stratification and consequently lowers the ΔT . Thus, increasing the mass flux can effectively mitigate the uneven temperature distribution in the horizontal tube.

IV. CONCLUSIONS AND PROSPECTS

This paper presents a numerical investigation of sCO_2 heat transfer in a horizontal tube. The ranges of tube diameter, pressure, mass flux, and heat flux are 8-12 mm, 10-20 MPa, 700-1300 kg/m²s, 66.7-300 kW/m², respectively. The main conclusions are summarized as follows:

- (1) For normal heat transfer (NHT) cases, the tube wall temperatures in the circumferential direction are almost uniform. The liquidlike region occupies the main area of the cross section. Due to the increasing specific heat capacity of liquid-like with rising temperature, the heat transfer coefficients increase in the flow direction on both the top generatrix and the bottom generatrix.
- (2) For heat transfer deterioration (HTD) cases, there are not only overshoot wall temperatures along the flow direction but also non-uniform wall temperatures in the circumferential direction. The temperature differences (ΔT) between the top generatrix

- and bottom generatrix are determined by the ratio of the vapor-like film thicknesses between the top generatrix and bottom generatrix, which first increases and then decreases in the flow direction. ΔT reaches 199.7 K, maximally.
- (3) The effect of tube diameter is analyzed based on the pseudo-boiling theory. Specifically, the heat transfer coefficient (HTC) at the top generatrix increases with decreasing tube diameter, while HTC at the bottom generatrix exhibits nonlinear variation with reducing tube diameter. However, HTCs at both top generatrix and bottom generatrix are dominated by supercritical *K* number, which characterizes the balance between evaporation momentum force and inertia force on vapor-like film to determine its thermal resistance.
- (4) The ΔT is determined by the ratio of the K number at the top generatrix to that at the bottom generatrix. Within the parameter ranges, ΔT decreases significantly with the reduction of diameter of the tube. In addition, ΔT reduces distinctly with increasing both pressure and mass flux for large tube. ΔT reduces effectively with increasing mass flux but changes slightly with rising pressure.

The above conclusions confirm that pseudo-boiling theory is a promising method to investigate supercritical heat transfer. It also

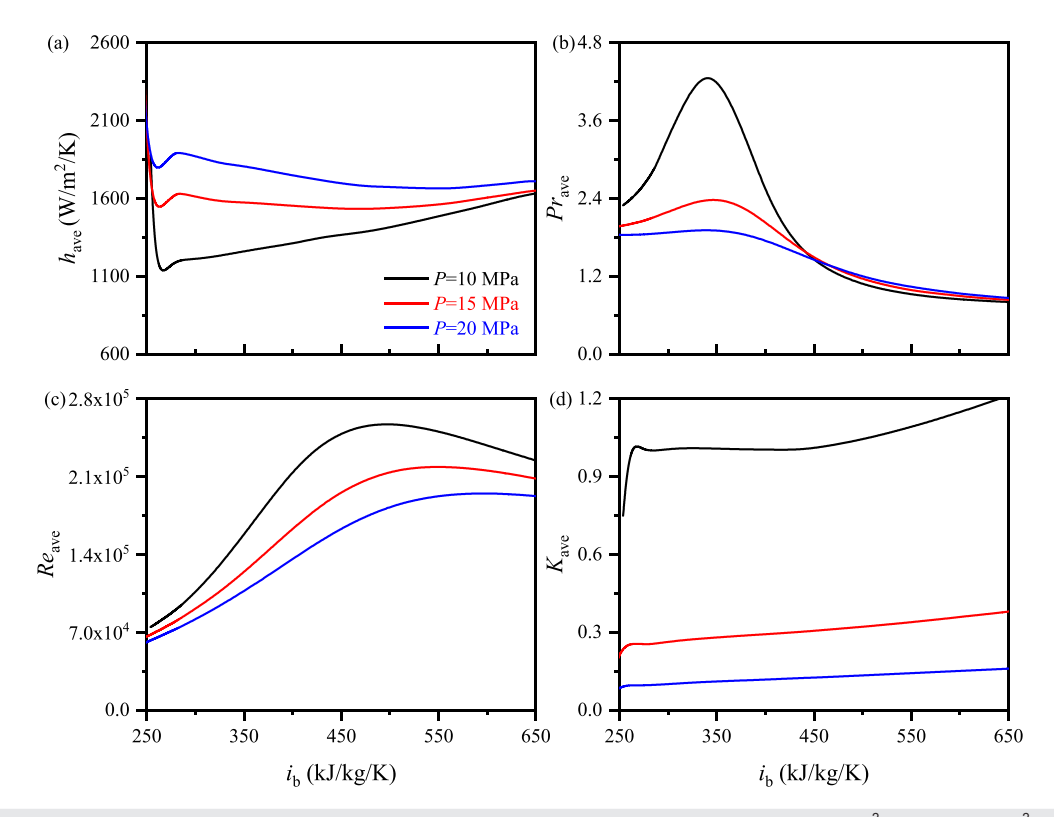


FIG. 12. Effect of pressure on the heat transfer performance and related dimensionless numbers in horizontal tube ($G = 700 \text{ kg/m}^2 \text{s}$, $q_{wi} = 300 \text{ kW/m}^2$): variation of (a) heat transfer coefficients h_{ave} , (b) Prandtl number Pr, (c) Reynolds number Re, and (d) supercritical K_{ave} number with bulk enthalpy i_b under different pressures.

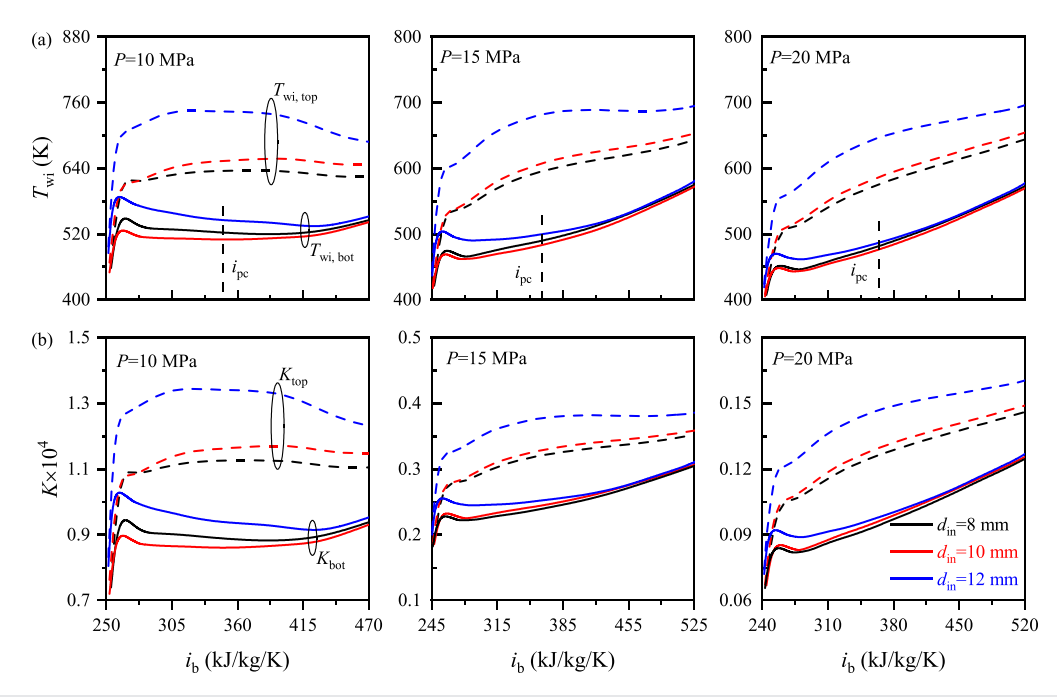


FIG. 13. Effect of tube diameter on the heat transfer performance at different pressure ($G = 700 \text{ kg/m}^2 \text{s}$, $q_{wi} = 300 \text{ kW/m}^2$): variation of (a) inner wall temperature T_{wi} and (b) supercritical K number with bulk enthalpy i_b .

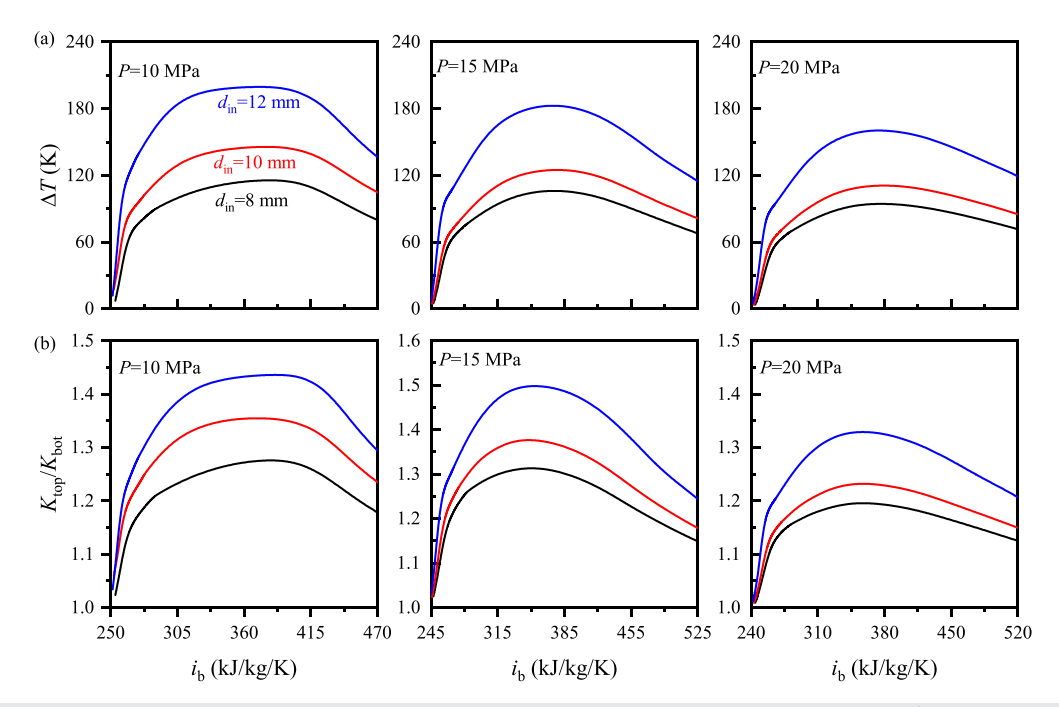


FIG. 14. Effect of tube diameter on the heat transfer difference between top and bottom generatrix at different pressures ($G = 700 \text{ kg/m}^2 \text{s}$, $q_{wi} = 300 \text{ kW/m}^2$): variation of (a) the wall temperature difference between the top and bottom generatrix ΔT and (b) supercritical $K_{\text{top}}/K_{\text{bot}}$ with bulk enthalpy i_{b} .

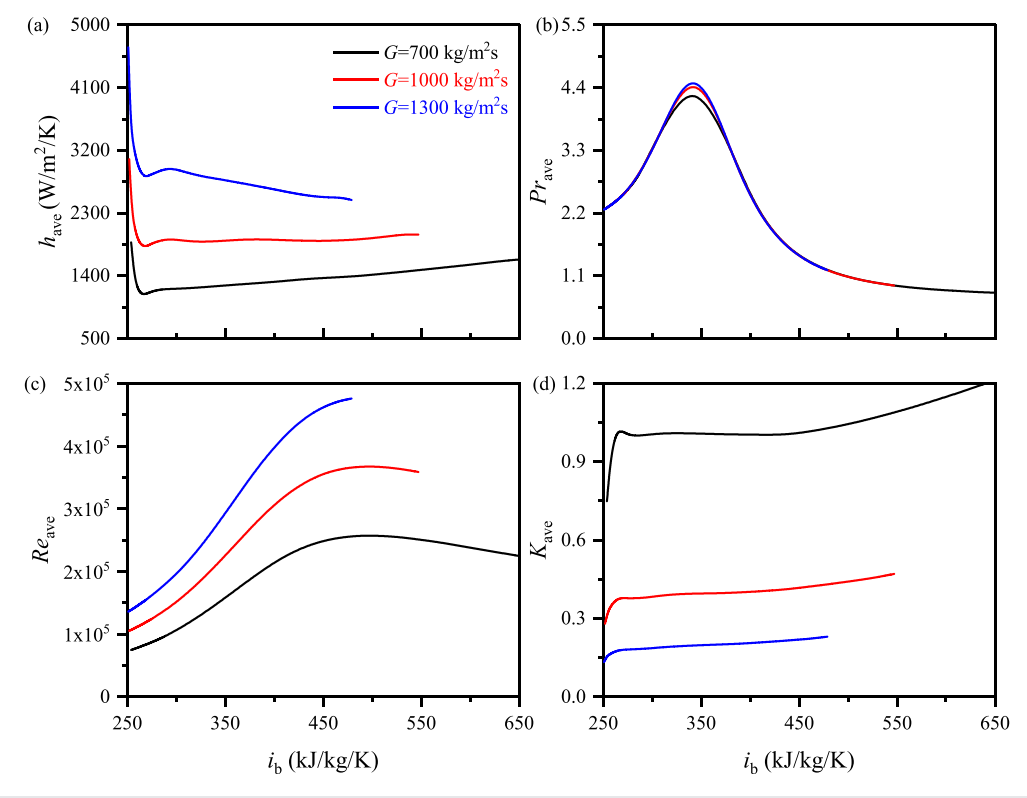


FIG. 15. Effect of mass flux on the heat transfer performance and related dimensionless numbers in horizontal tube (P = 10 MPa, $q_{wi} = 300 \text{ kW/m}^2$): variation of (a) heat transfer coefficients h_{ave} , (b) Prandtl number Pr, (c) Reynolds number Re, and (d) supercritical K_{ave} number with bulk enthalpy i_{b} under different mass fluxs.

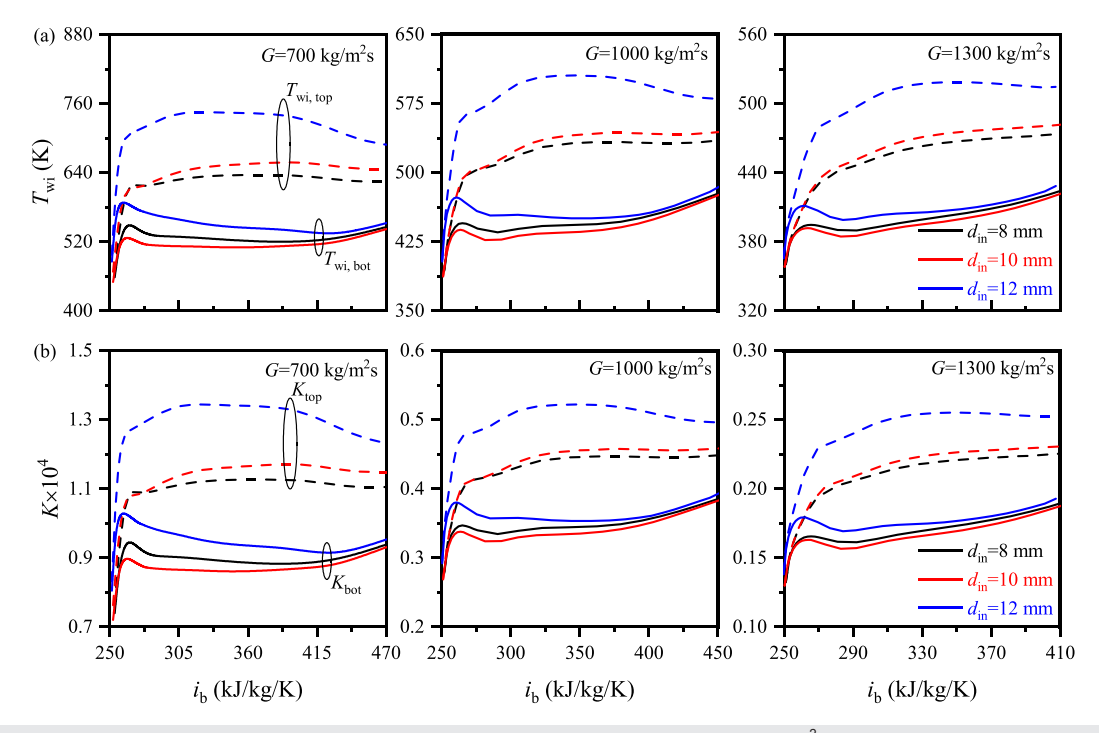


FIG. 16. Effect of tube diameter on the heat transfer performance at different mass flux (P = 10 MPa, $q_{wi} = 300 \text{ kW/m}^2$): variation of (a) inner wall temperature T_{wi} and (b) supercritical K number with bulk enthalpy i_b .

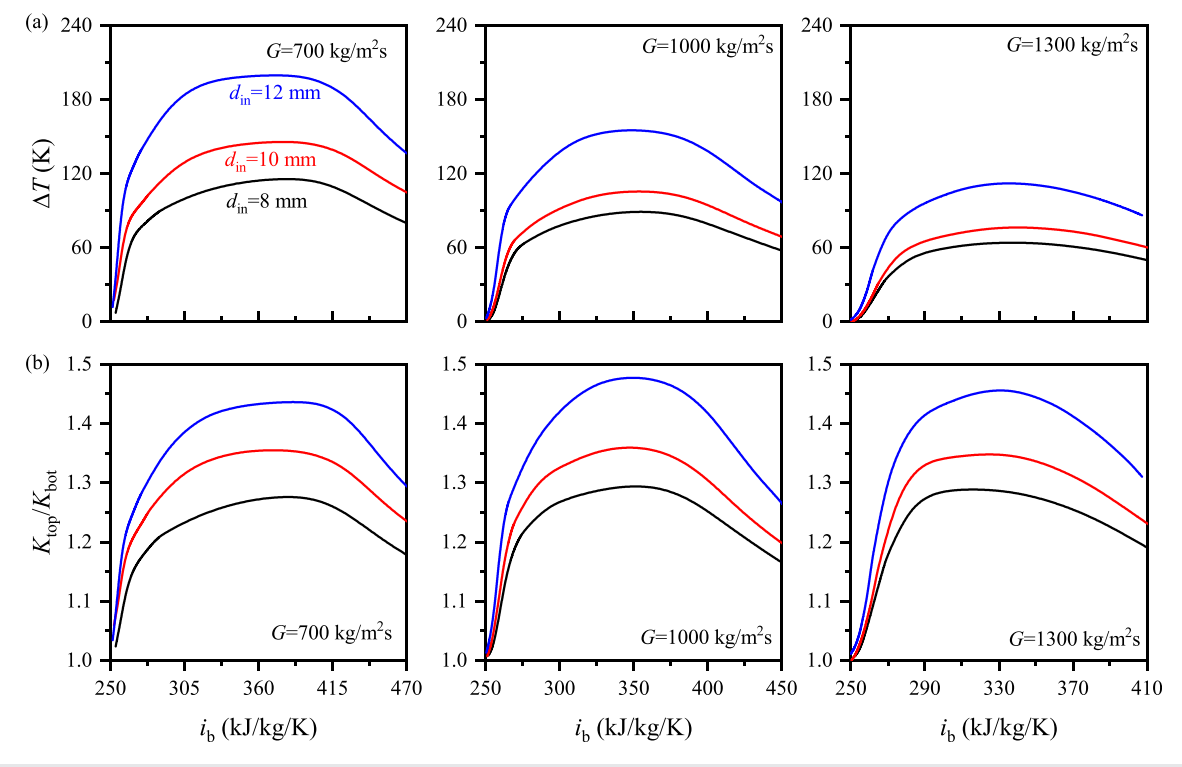


FIG. 17. Effect of tube diameter on the heat transfer difference between top and bottom generatrix at different mass flux (P = 10 MPa, $q_{wi} = 300 \text{ kW/m}^2$): variation of (a) the wall temperature difference between the top and bottom generatrix ΔT and (b) supercritical K_{top}/K_{bot} with bulk enthalpy i_b .

provides some meaningful results for the safety design of sCO₂ heat exchangers. However, more investigation needs to be performed in the future, including the following issues:

- (1) This paper focuses on the heat exchanger tube in advanced sCO₂ power systems. Various supercritical fluids in a tube with a wide diameter range need more investigations based on pseudoboiling theory for other applications such as micro-channel coolers of aero-engine and automobile air-conditioning.
- (2) This paper adopts the control variable method to clearly reveal the influences of tube diameter, pressure, and mass flux on supercritical heat transfer, respectively. It is recommended to study more combined influence of multiple factors on supercritical heat transfer in future investigations.
- (3) The uniformity of wall temperature is the key to keeping safe of supercritical heat exchanger. Although a small tube size is helpful to reduce the uniformity in the circumferential direction. The temperature differences between the top generatrix and bottom generatrix ΔT still remain relatively high. Other active modulation methods are desired.

ACKNOWLEDGMENTS

The authors acknowledge the support from the National Natural Science Foundation of China (Nos. 52130608 and 52176153). The authors also thank the organization of the "The 2024 International Conference on Supercritical CO₂ Power Cycle and Comprehensive Energy Systems" by the "The Institute of Engineering Thermophysics, Chinese Academy of Sciences" in "Shanghai and China" held over "September 20-24, 2024" for creating the platform at which, and for bringing together the audience to which, this work was first presented.

AUTHOR DECLARATIONS

Conflict of Interest

The authors have no conflicts to disclose.

Author Contributions

Bowen Yu: Formal analysis (lead); Investigation (lead); Methodology (lead); Software (lead); Writing - review & editing (lead). Jian Xie: Conceptualization (lead); Funding acquisition (lead); Writing - original draft (lead). Jinliang Xu: Project administration (lead); Resources (lead); Supervision (lead). Qiuru Dong: Data curation (lead); Visualization (equal). Liangyuan Cheng: Validation (lead); Visualization (equal).

DATA AVAILABILITY

The data that support the findings of this study are available from the corresponding author upon reasonable request.

NOMENCLATURE

- Specific heat capacity (J/kg K)
- Inner diameter of the tube (m) $d_{\rm in}$
- Outer diameter of the tube (m)
 - Mass flux $(kg/m^2 s)$
 - Gravitational acceleration (m/s²)
 - Heat transfer coefficient (W/m²K)

- Enthalpy (kJ/kg)
- Turbulent energy (m^2/s^2)
- Non-dimensional number K
- Mass flow rate (kg/s)
- P Pressure (MPa)
- PrPrandtl number
- Heat flux (W/m²)
- Radius (m) r
- Reynolds number Re
- Thermal resistance (m² K/W) $R_{\rm VI}$
- SBOSupercritical boiling number
 - TTemperature (K)
- T^{-} The onset of pseudo-boiling temperature (K)
- T^{+} The termination of pseudo-boiling temperature (K)
- ΔT Wall temperature difference (K)
- The distance from the top wall surface to the center of the y_{top}
- The distance from the bottom wall surface to the center of the tube (m)

Greek symbols

- Vapor-like film thickness (m)
- Thermal conductivity (W/m K)
- Kinematic viscosity (Pas)
- Polar angle (°)
- Density (kg/m³)

Subscripts

- ave Average
- Bulk fluid Ъ
- bot Bottom generatrix
- Experimental data exp
 - in Inlet

out

- Maximum value max Outlet
 - Pseudo-critical pc
- Simulated value pre
- Solid Top generatrix top
- Inner wall wi
- Outer wall

Abbreviations

- HTC Heat transfer coefficient
- HTD Heat transfer deterioration
 - LL Liquid-like
- Normal heat transfer NHT
- sCO₂ Supercritical carbon dioxide
- TPL Two-phase-like
- VLVapor-like

REFERENCES

¹Ž. Knez, E. Markočič, M. Leitgeb, M. Primožič, M. Knez Hrnčič, and M. Škerget, "Industrial applications of supercritical fluids: A review," Energy 77,

- ²C. R. Zhao, Z. Zhang, P. X. Jiang, R. N. Xu, and H. L. Bo, "Influence of channel scale on the convective heat transfer of CO₂ at supercritical pressure in vertical tubes," Int. J. Heat Mass Transfer 126, 201 (2018).
- ³J. H. Song, H. Y. Kim, H. Kim, and Y. Y. Bae, "Heat transfer characteristics of a supercritical fluid flow in a vertical pipe," J. Supercrit. Fluids 44, 164 (2008).
- ⁴H. Kim, H. Y. Kim, J. H. Song, and Y. Y. Bae, "Heat transfer to supercritical pressure carbon dioxide flowing upward through tubes and a narrow annulus passage," Prog. Nucl. Energy 50, 518 (2008).
- passage," Prog. Nucl. Energy 50, 518 (2008).

 5Y. Y. Bae, H. Y. Kim, and D. J. Kang, "Forced and mixed convection heat transfer to supercritical CO₂ vertically flowing in a uniformly-heated circular tube," Exp. Therm. Fluid Sci. 34, 1295 (2010).
- ⁶H. Zahlan, D. Groeneveld, and S. Tavoularis, "Measurements of convective heat transfer to vertical upward flows of CO₂ in circular tubes at near-critical and supercritical pressures," Nucl. Eng. Des. 289, 92 (2015).
- ⁷K. Wang, Z. D. Zhang, M. J. Li, and C. H. Min, "A coupled optical-thermal-fluid-mechanical analysis of parabolic trough solar receivers using supercritical CO₂ as heat transfer fluid," Appl. Therm. Eng. 183, 116154 (2021).
- ⁸S. M. Liao and T. S. Zhao, "Measurements of heat transfer coefficients from supercritical carbon dioxide flowing in horizontal mini/micro channels," J. Heat Transfer 124, 413 (2002).
- ⁹L. Wang, Y. C. Pan, J. Der Lee, Y. Wang, B.-R. Fu, and C. Pan, "Experimental investigation in the local heat transfer of supercritical carbon dioxide in the uniformly heated horizontal miniature tubes," Int. J. Heat Mass Transfer 159, 120136 (2020).
- ¹⁰L. Cheng, J. Xu, Q. Wang, and X. Dong, "The influence of tube diameter parameters on the flow resistance and heat transfer characteristics of supercritical CO₂ in horizontal tubes," Appl. Therm. Eng. 241, 122361 (2024).
- ¹¹S. Yu, H. Li, X. Lei, Y. Feng, Y. Zhang, H. He, and T. Wang, "Experimental investigation on heat transfer characteristics of supercritical pressure water in a horizontal tube," Exp. Therm. Fluid Sci. 50, 213 (2013).
- ¹²J. Wang, K. Qin, J. Gong, and K. Hooman, "Turbulent heat transfer of highly buoyant supercritical CO₂ flow in various horizontal pipes," Int. Commun. Heat Mass Transfer 133, 105939 (2022).
- ¹³J. D. Jackson, "Models of heat transfer to fluids at supercritical pressure with influences of buoyancy and acceleration," Appl. Therm. Eng. 124, 1481 (2017).
- ¹⁴H. S. Zhang, X. J. Zhu, B. G. Zhu, J. L. Xu, and H. Liu, "Effects of buoyancy and acceleration on heat transfer of supercritical CO₂ flowing in tubes," Acta Phys. Sin. 69, 064401 (2020).
- ¹⁵D. Huang and W. Li, "A brief review on the buoyancy criteria for supercritical fluids," Appl. Therm. Eng. 131, 977 (2018).
- ¹⁶D. Huang, Z. Wu, B. Sunden, and W. Li, "A brief review on convection heat transfer of fluids at supercritical pressures in tubes and the recent progress," Appl. Energy 162, 494 (2016).
- ¹⁷G. G. Simeoni, T. Bryk, F. A. Gorelli, M. Krisch, G. Ruocco, M. Santoro, and T. Scopigno, "The Widom line as the crossover between liquid-like and gas-like behaviour in supercritical fluids," Nat. Phys. 6, 503 (2010).
- ¹⁸X. He, J. Xu, X. Yu, and J. Xie, "Distinguishing evaporation-like and boiling-like modes of pseudo-boiling in supercritical pressures," Int. J. Heat Mass Transfer 214, 124417 (2023).
- ¹⁹F. Maxim, C. Contescu, P. Boillat, B. Niceno, K. Karalis, A. Testino, and C. Ludwig, "Visualization of supercritical water pseudo-boiling at Widom line crossover," Nat. Commun. 10, 4114 (2019).
- ²⁰D. T. Banuti, "Crossing the Widom-line—Supercritical pseudo-boiling," J. Supercrit, Fluids 98, 12 (2015).
- ²¹X. Li and Y. Jin, "Thermodynamic crossovers in supercritical fluids," Proc. Natl. Acad. Sci. U. S. A. 121, e2400313121 (2024).
- ²²Y. H. Fan, G. H. Tang, Q. Sheng, X. L. Li, and D. L. Yang, "S-CO₂ cooling heat transfer mechanism based on pseudo-condensation and turbulent field analysis," Energy 262, 125470 (2023).
- ²³X. L. Li, X. Y. Yu, P. T. Liu, Y. H. Fan, D. L. Yang, and G. H. Tang, "S-CO₂ flow in vertical tubes of large-diameter: Experimental evaluation and numerical exploration for heat transfer deterioration and prevention," Int. J. Heat Mass Transfer 216, 124563 (2023).
- ²⁴P. M. Tripathi and S. Basu, "Insights into the dynamics of supercritical water flow using a two-phase approach," Phys. Fluids 33, 043304 (2021).

- ²⁵B. Yuan, W. Wang, G. Xin, and W. Du, "Numerical analysis of heat transfer characteristics to supercritical CO₂ in a vertical mini-channel: Transition and pseudo-boiling," J. Therm. Sci. 33, 101 (2024).
 ²⁶N. Longmire and D. T. Banuti, "Onset of heat transfer deterioration caused by
- ²⁶N. Longmire and D. T. Banuti, "Onset of heat transfer deterioration caused by pseudo-boiling in CO₂ laminar boundary layers," Int. J. Heat Mass Transfer 193, 122957 (2022).
- ²⁷Q. Wang, X. Ma, J. Xu, M. Li, and Y. Wang, "The three-regime-model for pseudo-boiling in supercritical pressure," Int. J. Heat Mass Transfer 181, 121875 (2021).
- ²⁸B. Zhu, J. Xu, C. Yan, and J. Xie, "The general supercritical heat transfer correlation for vertical up-flow tubes: K number correlation," Int. J. Heat Mass Transfer 148, 119080 (2020).
- ²⁹B. Zhu, J. Xu, X. Wu, J. Xie, and M. Li, "Supercritical 'boiling' number, a new parameter to distinguish two regimes of carbon dioxide heat transfer in tubes," Int. J. Therm. Sci. 136, 254 (2019).
- 30 J. Xu, H. Zhang, B. Zhu, and J. Xie, "Critical supercritical-boiling-number to determine the onset of heat transfer deterioration for supercritical fluids," Sol. Energy 195, 27 (2020).
- ³¹B. Zhu, J. Xu, H. Zhang, J. Xie, and M. Li, "Effect of non-uniform heating on sCO₂ heat transfer deterioration," Appl. Therm. Eng 181, 115967 (2020).
- ³²L. Cheng, Q. Wang, and J. Xu, "Supercritical heat transfer of CO₂ in horizontal tube emphasizing pseudo-boiling and stratification effects," Int. J. Heat Mass Transfer 220, 124953 (2024).
- ³³L. Cheng, J. Xu, W. Cao, K. Zhou, and G. Liu, "Supercritical carbon dioxide heat transfer in horizontal tube based on the Froude number analysis," Energy 294, 130980 (2024).
- ³⁴H. Zhang, J. Xu, Q. Wang, and X. Zhu, "Multiple wall temperature peaks during forced convective heat transfer of supercritical carbon dioxide in tubes," Int. J. Heat Mass Transfer 172, 121171 (2021).
- 35H. Pu, H. Chang, J. Wang, Y. Shang, M. Dong, and S. Li, "Experimental investigation and analysis of convective heat transfer to supercritical pressure aviation kerosene RP-3 in vertical miniature tubes based on the pseudo-boiling theory," Appl. Therm. Eng. 219, 119651 (2023).
- 36 W. Dong, W. Wei, L. Zhao, L. Zhang, T. Zhou, and J. Ba, "The impact of the pseudo-boiling on the thermal behaviors of supercritical CO₂," Numer. Heat Transfer, Part A 84, 238 (2023).
- ³⁷B. Yu and J. Xu, "Numerical simulation of flow heat transfer of ultra-high parameter CO₂ in horizontal tubes," in Proceedings of the CSEE, 2025.
- ³⁸ANSYS, ANSYS Fluent 19.2 Solver Theory Guide (ANSYS, Inc., 2019).
- ⁵⁹C. Yan, J. Shi, S. Zhang, X. Zhang, and Q. Chen, "Investigation on heat transfer of supercritical CO₂/Xe mixture crossing pseudo-critical temperature cooled in a horizontal circular tube," Appl. Therm. Eng. 257, 124245 (2024).
- ⁴⁰E. W. Lemmon, M. L. Huber, and M. O. Mclinden, NIST Standard Reference Database 23: Reference Fluid Thermodynamic and Transport Properties-REFPROP, Version 9.0 (NIST NSRDS, 2010).
- ⁴¹X. Peng, D. Wang, G. Wang, Y. Yang, and S. Xiang, "Numerical investigation on the heating performance of a transcritical CO₂ vapor-injection heat pump system," Appl. Therm. Eng. 166, 114656 (2020).
- ⁴²J. Xu, E. Sun, M. Li, H. Liu, and B. Zhu, "Key issues and solution strategies for supercritical carbon dioxide coal fired power plant," Energy 157, 227 (2018).
- ⁴³Y. Qiu, M.-J. Li, Y.-L. He, and W.-Q. Tao, "Thermal performance analysis of a parabolic trough solar collector using supercritical CO₂ as heat transfer fluid under nonuniform solar flux," Appl. Therm. Eng. 115, 1255 (2017).
- 44H. Yamaguchi, X. R. Zhang, K. Fujima, M. Enomoto, and N. Sawada, "Solar energy powered Rankine cycle using supercritical CO₂," Appl. Therm. Eng. 26, 2345 (2006)
- ⁴⁵B. Yu, J. Xie, J. Xu, and L. Cheng, "Numerical study on pseudo-boiling heat transfer of supercritical CO₂ in horizontal tube," Int. J. Heat Mass Transfer 244, 126981 (2025).
- ⁴⁶C. Yan, J. Xu, S. Wang, and G. Liu, "Numerical study of convective heat transfer to supercritical CO₂ in vertical heated tubes," Int. Commun. Heat Mass Transfer 137, 106242 (2022).
- ⁴⁷Y. Zhang, X. Zhang, C. Yan, W. Wu, and E. Gao, "Numerical investigation on characteristics of supercritical CO₂ heat transfer in vertical circular tubes with circumferentially half-side heating," J. Therm. Sci. 33, 1744 (2024).